Article

Timoshenko Beam Theory: First-Order Analysis, Second-Order Analysis, Stability, and Vibration Analysis Using the Finite Difference Method

Valentin Fogang

Abstract: This paper presents an approach to the Timoshenko beam theory (TBT) using the finite difference method (FDM). The TBT covers cases associated with small deflections based on shear deformation considerations, whereas the Euler–Bernoulli beam theory neglects shear deformations. The FDM is an approximate method for solving problems described with differential or partial differential equations. It does not involve solving differential equations; equations are formulated with values at selected points of the structure. The model developed in this paper consists of formulating partial differential equations with finite differences and introducing new points (additional or imaginary points) at boundaries and positions of discontinuity (concentrated loads or moments, supports, hinges, springs, brutal change of stiffness). The introduction of additional points allows satisfying boundary and continuity conditions. First-order, second-order, and vibration analyses of structures were conducted with this model. Efforts, displacements, stiffness matrices, buckling loads, and vibration frequencies were determined. In addition, tapered beams were analyzed (e.g., element stiffness matrix, second-order analysis, and vibration analysis). Finally, the direct time integration method (DTIM) was presented. The FDM-based DTIM enabled the analysis of forced vibration of structures, considering the damping. The efforts and displacements could be determined at any time.

Keywords: Timoshenko beam; finite difference method; additional points; element stiffness matrix; tapered beam; second-order analysis; vibration analysis; direct time integration method

Corresponding author: Valentin Fogang

Civil Engineer

C/o BUNS Sarl P.O Box 1130 Yaounde Cameroon

E-mail: valentin.fogang@bunscameroun.com

ORCID iD https://orcid.org/0000-0003-1256-9862

1. Introduction

This paper describes the application of Fogang's model [1] based on the finite difference method, used for the Euler–Bernoulli beam, to the Timoshenko beam. First-order analysis of the Timoshenko beam is routinely performed; the principle of virtual work yields accurate results and is easy to apply. However, second-order and vibration analyses of the Timoshenko beam cannot be modeled using the principle of virtual work. Various studies have focused on the analysis of Timoshenko beams. Kindelan et al. [2] presented a method of obtaining optimal finite difference formulas that maximize their frequency range of validity. Both conventional and staggered equispaced stencils for first and

 doi:10.20944/preprints202105.0252.v1

second derivatives were considered. Onyia et al. [3] presented a finite element formulation to determine the critical buckling load of the unified beam element that is free from shear locking using the energy method; the technique provides a unified approach to performing stability analysis of beams with any end conditions. Timoshenko and Gere [4] proposed formulas to account for shear stiffness by calculating buckling loads of associated Euler–Bernoulli beams. Hu et al. [5] used matrix structural analysis to derive a closed-form solution of the second-order element stiffness matrix; the buckling loads of single-span beams were also determined. Fogang [6] presented a material law describing the relationship between curvature, bending moment, and shear force; based on this material law, closed-form expressions of efforts and deformations are derived, as well as first- and second-order element stiffness matrices. Mwabora et al. [7] considered numerical solutions for static and dynamic stability parameters of an axially loaded uniform beam resting on simply supported foundations using the finite difference method (FDM), where a central difference scheme was developed. Soltani et al. [8] applied the FDM to evaluate natural frequencies of non-prismatic beams with different boundary conditions and resting on variable one- or two-parameter elastic foundations. Boreyri et al. [9] analyzed the free vibration of a new type of tapered beam, with exponentially varying thickness, resting on a linear foundation; the solution was based on a semi-analytical technique, the differential transform method. Torabi et al. [10] presented an exact closed-form solution for free vibration analysis of Euler–Bernoulli conical and tapered beams carrying any desired number of attached masses; the concentrated masses were modeled by Dirac's delta functions. Fogang [11] presented a material law describing the relationship between curvature, bending moment, shear force, and natural frequency; based on this material law closed-form expressions of dynamic first- and second-order element stiffness matrices are derived and natural frequencies are determined. Yesilce et al. [12] studied the free vibration of a multi-span Timoshenko beam carrying multiple spring–mass systems; natural frequencies were calculated using the secant method, and mode shapes were presented in graphs. Katsikadelis [13] presented a direct time integration method for solving the equations of motion describing the dynamic response of structural linear and nonlinear multi-degree-of-freedom systems; the method was also applied to equations with variable coefficients. Ghannadiasl [14] used Green functions to analytically solve the case of beams with various boundary conditions, resting on an elastic Winkler foundation and subjected to an axial load; the Green function method was used to evaluate the free vibration of the Timoshenko beam. Kruszewski [15] presented a theoretical analysis of the effect of transverse shear and rotary inertia on the natural frequencies of a uniform cantilevered Timoshenko beam. Soltani [16] developed a semi-analytical technique to investigate the free bending vibration behavior of an axially functionally graded non-prismatic Timoshenko beam subjected to a point force at both ends, based on the power series expansion.

Classical analysis of the Timoshenko beam involves solving the governing equations (i.e., statics and material) that are expressed via means of differential equations, considering boundary and continuity conditions. However, solving differential equations may be difficult in the presence of an axial force (or external distributed axial forces), an elastic Winkler foundation, a Pasternak foundation, or damping (by vibration analysis). In traditional analysis using the FDM, points outside the beam are not considered. The boundary conditions are applied at the beam's ends, not the governing equations. The non-application of governing equations at the beam's ends leads to inaccurate results, making the FDM less useful compared with other numerical methods, such as the finite element method. This paper presented a model based on the FDM. This model consisted of formulating differential equations (statics and material relation) with finite differences and introducing new points (additional or imaginary points) at boundaries and at positions of discontinuity (concentrated loads or moments, supports, hinges, springs, and brutal change of stiffness). The introduction of additional points allowed us to satisfy boundary and continuity conditions. First-order, second-order, and vibration analyses of structures were also conducted using the model.

2. Materials and methods

2.1 First-order analysis

2.1.1 Statics

The sign convention adopted for the loads, bending moments, shear forces, and displacements is illustrated in Figure 1.

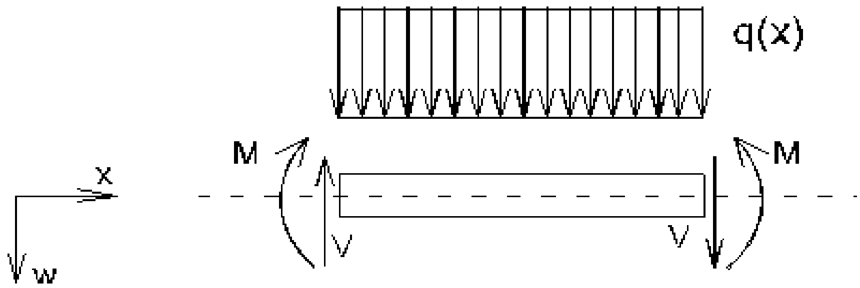

Figure 1. Sign convention for loads, bending moments, shear forces, and displacements.

Specifically, M(x) is the bending moment in the section, V(x) is the shear force, w(x) is the deflection, and q(x) is the distributed load in the positive downward direction.

In first-order analysis the equations of static equilibrium on an infinitesimal element are as follows:

$$\frac{dV(x)}{dx} - k(x)w(x) = -q(x) \tag{1a}$$

$$\frac{dM(x)}{dx} - V(x) = 0, \tag{1b}$$

where k(x) is the stiffness of the elastic Winkler foundation. Substituting Equation (1b) into Equation (1a) yields

$$\frac{d^2M(x)}{dx^2} - k(x)w(x) = -q(x) \tag{2}$$

According to Timoshenko beam theory, the bending moment and shear force are related to the deflection and rotation (positive in clockwise) of the cross section φ(x), as follows:

$$M(x) = -EI\frac{d\varphi(x)}{dx} \tag{3}$$

$$V(x) = \kappa GA \times \left(\frac{dw(x)}{dx} - \varphi(x)\right) \tag{4}$$

where E is the elastic modulus, I is the second moment of area, κ is the shear correction factor, G is the shear modulus, and A is the cross-sectional area.

In the case of a uniform beam, substituting Equations (3) and (4) into Equations (1a) and (1b) yields

$$\kappa GA\times\left(\frac{d^2w(x)}{dx^2}-\frac{d\varphi(x)}{dx}\right)-kw(x)=-q(x) \tag{5a}$$

$$EI\frac{d^2\varphi(x)}{dx^2}+\kappa GA\times\left(\frac{dw(x)}{dx}-\varphi(x)\right)=0 \tag{5b}$$

In the case of a tapered beam, substituting Equations (3) and (4) into Equations (1a) and (1b) yields

$$\frac{d\kappa GA(x)}{dx}\times\left(\frac{dw(x)}{dx}-\varphi(x)\right)+\kappa GA(x)\times\left(\frac{d^2w(x)}{dx^2}-\frac{d\varphi(x)}{dx}\right)-kw(x)=-q(x) \tag{6a}$$

$$\frac{dEI(x)}{dx}\times\frac{d\varphi(x)}{dx}+EI(x)\frac{d^2\varphi(x)}{dx^2}+\kappa GA(x)\times\left(\frac{dw(x)}{dx}-\varphi(x)\right)=0 \tag{6b}$$

Fogang [6] presented the following formulas for a uniform and a tapered beam, respectively:

$$\frac{d^2w(x)}{dx^2}+\frac{M(x)}{EI}-\frac{1}{\kappa GA}\frac{d^2M(x)}{dx^2}=0, \tag{6c}$$

$$\frac{d^2w(x)}{dx^2}+\frac{M(x)}{EI(x)}-\frac{1}{\kappa GA(x)}\frac{d^2M(x)}{dx^2}+\frac{1}{(\kappa GA(x))^2}\times\frac{d\kappa GA(x)}{dx}\times\frac{dM(x)}{dx}=0\ , \tag{6d}$$

Differentiating Equation (6c) twice with respect to *x* and combining the result with Equation (2) yields the following widely known formula for a uniform beam without Winkler foundation:

$$EI\frac{d^4w(x)}{dx^4}=q(x)-\frac{EI}{\kappa GA}\frac{d^2q(x)}{dx^2} \tag{6e}$$

In the presence of an elastic Winkler foundation, Equation (6e) becomes

$$EI\frac{d^4w(x)}{dx^4}-\frac{EI}{\kappa GA}\frac{d^2\left(k(x)w(x)\right)}{dx^2}+k(x)w(x)=q(x)-\frac{EI}{\kappa GA}\frac{d^2q(x)}{dx^2} \tag{6f}$$

For a uniform beam, the bending moment, the shear force, and the rotation of the cross section are derived using Equations (6c) and (2), Equation (1b), and Equation (4), respectively, as follows:

$$M(x)=-EI\frac{d^2w(x)}{dx^2}+\frac{EI}{\kappa GA}k(x)w(x)-\frac{EI}{\kappa GA}p(x) \tag{6g}$$

$$V(x)=-EI\frac{d^3w(x)}{dx^3}+\frac{EI}{\kappa GA}\frac{d\left(k(x)w(x)\right)}{dx}-\frac{EI}{\kappa GA}\frac{dp(x)}{dx} \tag{6h}$$

$$\varphi(x)=\frac{dw(x)}{dx}+\frac{EI}{\kappa GA}\frac{d^3w(x)}{dx^3}-\frac{EI}{(\kappa GA)^2}\frac{d\left(k(x)w(x)\right)}{dx}+\frac{EI}{(\kappa GA)^2}\frac{dp(x)}{dx} \tag{6i}$$

Hence, a W–Φ FDM approximation (Equations (5a)-(6b)), an M–W FDM approximation (Equations (2) and (6c-d)), and a W FDM approximation (Equations (6e-i)) can be considered.

2.1.2 FDM Formulation of equations, efforts, deformations, and loadings

2.1.2.1 Fundamentals of FDM

Figure 2 shows a segment of a beam having equidistant points with grid spacing h.

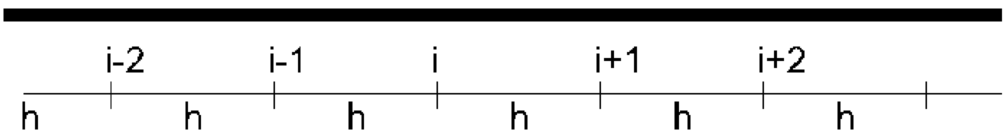

Figure 2. Beam with equidistant points.

Equations (5a)-(6d) have a second-order derivative; consequently, the deflection, rotation, and moment curves w(x), φ(x) and M(x), respectively, are approximated around the point of interest i as second-degree polynomials.

Thus, curves w(x) and φ(x) can be described with the deflections values at equidistant grid points:

$$w(x) = w_{i-1} \times f_{i-1}(x) + w_i \times f_i(x) + w_{i+1} \times f_{i+1}(x) \tag{7a}$$

The shape functions $f_j(x)$ (j = i-1, i, i+1) can be expressed using Lagrange polynomials:

$$f_j(x) = \prod_{\substack{k=i-1 \\ k \neq j}}^{i+1} \frac{x - x_k}{x_j - x_k} \tag{7b}$$

Thus, a three-point stencil is used to write finite difference approximations to derivatives at grid points. The derivatives (S(x) representing w(x) or φ(x)) at **i** are expressed with deflection values at points i-1, i, and i+1.

$$\left.\frac{d^2S(x)}{dx^2}\right|_i = \frac{S_{i-1} - 2S_i + S_{i+1}}{h^2} \quad \text{(8a)} \qquad \left.\frac{dS(x)}{dx}\right|_i = \frac{-S_{i-1} + S_{i+1}}{2h} \quad \text{(8b)}$$

Equation (6e) has a fourth-order derivative, and the deflection curve is consequently approximated around the point of interest i as a fourth-degree polynomial. Thus, a five-point stencil is used to write finite difference approximations to derivatives at grid points. The derivatives at **i** are expressed with deflection values at points i-2, i-1, i, i+1, and i+2.

$$\left.\frac{d^4w}{dx^4}\right|_i = \frac{w_{i-2} - 4w_{i-1} + 6w_i - 4w_{i+1} + w_{i+2}}{h^4} \tag{8c}$$

$$\left.\frac{d^3w}{dx^3}\right|_i = \frac{-w_{i-2} + 2w_{i-1} - 2w_{i+1} + w_{i+2}}{2h^3} \tag{8d}$$

$$\left.\frac{d^2w}{dx^2}\right|_i = \frac{-w_{i-2} + 16w_{i-1} - 30w_i + 16w_{i+1} - w_{i+2}}{12h^2} \tag{8e}$$

$$\left.\frac{dw}{dx}\right|_i = \frac{w_{i-2} - 8w_{i-1} + 8w_{i+1} - w_{i+2}}{12h} \tag{8f}$$

Preprints (www.preprints.org) | NOT PEER-REVIEWED | Posted: 11 May 2021 doi:10.20944/preprints202105.0252.v1

2.1.2.2 Uniform beam within segments

2.1.2.2.1 W–Φ FDM approximation of a uniform beam

Let us consider a segment k of the beam (length l) having equidistant grid points with spacing h_k. The flexural and shear stiffness values in this beam segment are EI_k and κGA_k. α_r is the bending shear factor. A reference flexural stiffness EI_r and a reference shear stiffness κGA_r are introduced as follows:

$$EI_k = \beta_{Mk} \times EI_r \quad (9a)$$

$$\kappa GA_k = \beta_{Vk} \times \kappa GA_r \quad (9b)$$

$$\alpha_r = EI_r / \left(\kappa GA_r l^2\right) \quad (9c)$$

$$h_k = \beta_{lk} l \quad (9d)$$

$$W(x) = EI_r \times w(x) \quad (9e)$$

$$\Phi(x) = EI_r \times \varphi(x) \quad (9f)$$

Substituting Equations (8a)-(9f) into Equations (5a-b) yields the following governing equations:

$$\beta_{Vk} W_{i-1} - \left(2\beta_{Vk} + \alpha_r \beta_{lk}^2 \frac{k_i l^4}{EI_r}\right) W_i + \beta_{Vk} W_{i+1} + \frac{\beta_{Vk}}{2} h_k \Phi_{i-1} - \frac{\beta_{Vk}}{2} h_k \Phi_{i+1} = -\frac{\alpha_r}{\beta_{lk}^2} q_i h_k^4 \quad (10a)$$

$$-\frac{\beta_{Vk}\beta_{lk}^2}{2\alpha_r} W_{i-1} + \frac{\beta_{Vk}\beta_{lk}^2}{2\alpha_r} W_{i+1} + \beta_{Mk} h_k \Phi_{i-1} - \left(2\beta_{Mk} + \frac{\beta_{Vk}\beta_{lk}^2}{\alpha_r}\right) h_k \Phi_i + \beta_{Mk} h_k \Phi_{i+1} = 0 \quad (10b)$$

Substituting Equations (8b) and (9a-f) into Equations (3)-(4) yields the bending moment and shear force, as follows:

$$M_i = \beta_{Mk} \frac{\Phi_{i-1} - \Phi_{i+1}}{2h_k} \quad (11a)$$

$$V_i = \frac{\beta_{Vk}\beta_{lk}^2}{\alpha_r h_k^{\,3}} \left(-\frac{W_{i-1}}{2} + \frac{W_{i+1}}{2} - h_k \Phi_i\right) \quad (11b)$$

2.1.2.2.2 W FDM approximation of a uniform beam

Equation (6f) is the governing equation. The stiffness k(*x*) of the Winkler foundation is assumed constant in the beam segment and is denoted by k_k. Substituting Equations (8c), (8e), and (9a-e) into Equation (6f) yields the following FDM formulations of the governing equation

$$\beta_{Mk}\left(W_{i-2} - 4W_{i-1} + 6W_i - 4W_{i+1} + W_{i+2}\right) + K^* \frac{W_{i-2} - 16W_{i-1} + 30W_i - 16W_{i+1} + W_{i+2}}{12} W_{i-2}$$

$$+ \frac{k_k h_k^{\,4}}{EI_r} W_i = q_i h_k^{\,4} - \frac{\beta_{Mk}\alpha_r}{\beta_{Vk}\beta_{lk}^2} h_k^{\,6} \left.\frac{d^2 q(x)}{dx^2}\right|_i \quad (12a)$$

$$K^* = \frac{\beta_{Mk}\alpha_r}{\beta_{Vk}\beta_{lk}^2} \frac{k_k h_k^{\,4}}{EI_r} \qquad k_k = k_W \frac{EI_r}{l^4} \quad (12b)$$

Preprints (www.preprints.org) | NOT PEER-REVIEWED | Posted: 11 May 2021 doi:10.20944/preprints202105.0252.v1

The bending moment, the shear force, and the rotation of the cross section are calculated using Equations (6g), (8e), and (12b), Equations (6h), (8d), and (12b), and Equations (6i), (8f), and (8d) as follows:

$$M_i = \beta_{MK}\frac{W_{i-2}-16W_{i-1}+30W_i-16W_{i+1}+W_{i+2}}{12h_k^{\ 2}}+K^*\frac{W_i}{h_k^{\ 2}}-\frac{\beta_{Mk}\alpha_r}{\beta_{Vk}}l^2 p_i \tag{13a}$$

$$V_i = \beta_{MK}\frac{W_{i-2}-2W_{i-1}+2W_{i+1}-W_{i+2}}{2h_k^{\ 3}}+K^*\frac{W_{i-2}-8W_{i-1}+8W_{i+1}-W_{i+2}}{12h_k^{\ 3}}-\frac{\beta_{Mk}\alpha_r}{\beta_{Vk}}l^2\left.\frac{dp(x)}{dx}\right|_i \tag{13b}$$

$$\begin{aligned}EI_r\varphi(x) = {} & \left(1-\frac{\beta_{Mk}k_W\alpha_r^{\ 2}}{\beta_{Vk}^2}\right)\frac{W_{i-2}-8W_{i-1}+8W_{i+1}-W_{i+2}}{12h_k} \\ & +\frac{\beta_{Mk}\alpha_r}{\beta_{Vk}\beta_{lk}^2}\frac{-W_{i-2}+2W_{i-1}-2W_{i+1}+W_{i+2}}{2h_k}+\frac{\beta_{Mk}\alpha_r^{\ 2}}{\beta_{Vk}^2}l^4\left.\frac{dp(x)}{dx}\right|_i\end{aligned} \tag{13c}$$

2.1.2.2.3 M–W FDM approximation of a uniform beam

Equations (2) and (6c) are the governing equations. Applying Equations (8a-b) and (9a-e) in Equations (2) and (6c) yields the corresponding FDM expressions, as follows:

$$h_k^{\ 2}M_{i-1}-2h_k^{\ 2}M_i+h_k^{\ 2}M_{i+1}-\beta_{lk}^4\frac{k_i l^4}{EI_r}W_i \quad =-q_i h_k^{\ 4} \tag{13d}$$

$$\beta_{Mk}\left(W_{i-1}-2W_i+W_{i+1}\right)-\frac{\beta_{Mk}\alpha_r}{\beta_{Vk}\beta_{lk}^2}\left(h_k^2M_{i-1}-2h_k^2M_i+h_k^2M_{i+1}\right)+h_k^2M_i=0 \tag{13e}$$

The shear force (Equations (1b) and (8b)) and the rotation of the cross section (Equations (1b), (4), (8b), and (9b-e)) are calculated as follows:

$$V_i=\frac{M_{i+1}-M_{i-1}}{2h_k} \tag{13f}$$

$$2EI_r\times\varphi_i=\frac{W_{i+1}-W_{i-1}}{h_k}-\frac{\alpha_r}{h_k\beta_{Vk}\beta_{lk}^2}\left(h_k^{\ 2}M_{i+1}-h_k^{\ 2}M_{i-1}\right) \tag{13g}$$

2.1.2.3 Tapered beam within segments

2.1.2.3.1 W–Φ FDM approximation of a tapered beam

The following parameters describing stiffnesses EI(x) and κGA(x) and their rate of change are defined.

$$EI(x)=\beta_M(x)\times EI_r \tag{14a}$$

$$\kappa GA(x)=\beta_V(x)\times\kappa GA_r \tag{14b}$$

$$\beta_M^{'}(x)=h_k\frac{d\beta_M(x)}{dx} \tag{14c}$$

$$\beta_V^{'}(x)=h_k\frac{d\beta_V(x)}{dx} \tag{14d}$$

Preprints (www.preprints.org) | NOT PEER-REVIEWED | Posted: 11 May 2021 doi:10.20944/preprints202105.0252.v1

Substituting Equations (9d) and (14a-d) into Equations (6a-b) yields the following governing equations for the tapered beam at position **i**:

$$\left(-\frac{\beta_{Vi}^{'}}{2}+\beta_{Vi}\right)W_{i-1}-\left(2\beta_{Vi}+\alpha_r\beta_{lk}^2\frac{k_i l^4}{EI_r}\right)W_i+\left(\frac{\beta_{Vi}^{'}}{2}+\beta_{Vi}\right)W_{i+1} \tag{15a}$$

$$+\frac{\beta_{Vi}}{2}h_k\Phi_{i-1}-\beta_{Vi}^{'}h_k\Phi_i-\frac{\beta_{Vi}}{2}h_k\Phi_{i+1}\qquad=-\frac{\alpha_r}{\beta_{lk}^2}q_i h_k^4$$

$$-\frac{\beta_{Vi}\beta_{lk}^2}{2\alpha_r}W_{i-1}+\frac{\beta_{Vi}\beta_{lk}^2}{2\alpha_r}W_{i+1}+\left(\beta_{Mi}-\frac{\beta_{Mi}^{'}}{2}\right)h_k\Phi_{i-1}-\left(2\beta_{Mi}+\frac{\beta_{Vi}\beta_{lk}^2}{\alpha_r}\right)h_k\Phi_i \tag{15b}$$

$$+\left(\frac{\beta_{Mi}^{'}}{2}+\beta_{Mi}\right)h_k\Phi_{i+1}\qquad=0$$

The bending moment and shear force are calculated using Equations (11a-b), β_{Mk} and β_{Vk} being replaced by β_{Mi} and β_{Vi}.

2.1.2.3.2 M–W FDM approximation of a tapered beam

Equations (2) and (6d) are the governing equations. Substituting Equations (8a-b), (9d), and (14a-d) into Equations (2) and (6d) yields Equation (13d) and the following equation:

$$\beta_{Mi}W_{i-1}-2\beta_{Mi}W_i+\beta_{Mi}W_{i+1}-\frac{\beta_{Mi}\alpha_r}{\beta_{Vi}\beta_{lk}^2}\left(1+\frac{\beta_{Vi}^{'}}{2\beta_{Vi}}\right)h_k^{\,2}M_{i-1}+\left(1+\frac{2\beta_{Mi}\alpha_r}{\beta_{Vi}\beta_{lk}^2}\right)h_k^{\,2}M_i \tag{16}$$

$$+\frac{\beta_{Mi}\alpha_r}{\beta_{Vi}\beta_{lk}^2}\left(\frac{\beta_{Vi}^{'}}{2\beta_{Vi}}-1\right)h_k^{\,2}M_{i+1}\qquad=0$$

Thus, Equations (13d) and (16) are the governing equations. The shear force and the rotation of the cross section are calculated using Equations (13f) and (13g), respectively. However, β_{Vk} is replaced by β_{Vi} in Equation (13g).

2.1.2.4 FDM approximation of q(*x*) and k(*x*)

Fogang [1] presented formulas to determine the FDM approximation of distributed loads and the stiffness of an elastic Winkler foundation. The FDM value q_i for position i being the left beam's end, an interior point on the beam, or the right beam's end is as follows:

$$q_i=\frac{1}{2h}\left[3\int_i^{i+1}q(x)dx-\int_{i+1}^{i+2}q(x)dx\right] \tag{17a}$$

$$q_i=\frac{1}{2h}\int_{i-1}^{i+1}q(x)dx \tag{17b}$$

$$q_i=\frac{1}{2h}\left[-\int_{i-2}^{i-1}q(x)dx+3\int_{i-1}^{i}q(x)dx\right] \tag{17c}$$

Preprints (www.preprints.org) | NOT PEER-REVIEWED | Posted: 11 May 2021 doi:10.20944/preprints202105.0252.v1

The application of Equations (17a-c) shows that for a linearly distributed load, $q_i = q(x_i)$.

At any point i, the stiffness of the elastic Winkler foundation, k_i, is calculated similarly to Equations (17a-c).

2.1.2.5 First derivatives of the stiffnesses EI(x) and κGA(x)

If analytical expressions of $\beta_M(x)$ (Equation (14a)) and $\beta_V(x)$ (Equation (14b)) are known, the corresponding first derivatives can be directly determined. If, instead, values are given at discrete points, the parameters β'_{Mi} (Equation (14c)) and β'_{Vi} (Equation (14d)) at position i can be calculated using Equations (18a-c), position i being considered the left beam's end, an interior point on the beam, or the right beam's end, respectively:

$$\beta'_{Mi} = h_k \left.\frac{d\beta_M(x)}{dx}\right|_i = \frac{-3\beta_{M\,i} + 4\beta_{M\,i+1} - \beta_{M\,i+2}}{2} \qquad (18a)$$

$$\beta'_{Mi} = h_k \left.\frac{d\beta_M(x)}{dx}\right|_i = \frac{-\beta_{M\,i-1} + \beta_{M\,i+1}}{2} \qquad (18b)$$

$$\beta'_{Mi} = h_k \left.\frac{d\beta_M(x)}{dx}\right|_i = \frac{\beta_{M\,i-2} - 4\beta_{M\,i-1} + 3\beta_{M\,i}}{2} \qquad (18c)$$

The parameter β'_V (Equation (14d)) is calculated similarly.

2.1.3 Analysis at positions of discontinuity

Positions of discontinuity are positions of application of concentrated external loads (force or moment), supports, hinges, springs, abrupt change in cross section, positions where EI(x) and κGA(x) are not differentiable, and change in grid spacing.

2.1.3.1 Uniform beam within segments

In the case of concentrated loads (force P and moment M^*) applied at point i (Figure 3), the beam has a uniform cross section within segments. At point i, an abrupt change in cross section and a change in grid spacing are assumed.

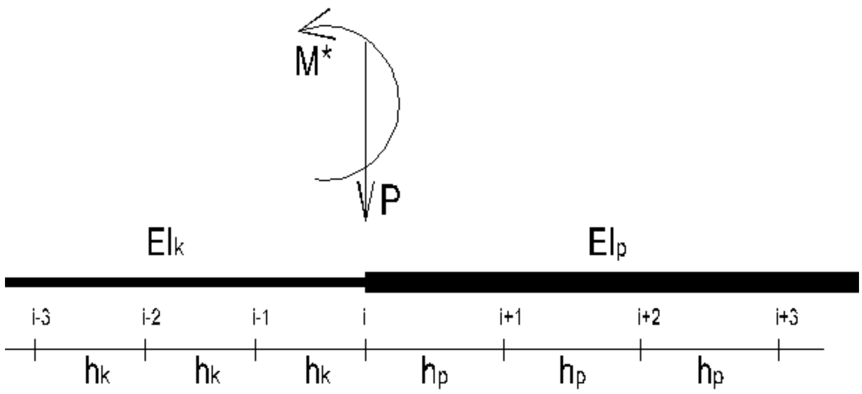

Figure 3. Beam with concentrated loads.

Preprints (www.preprints.org) | NOT PEER-REVIEWED | Posted: 11 May 2021 doi:10.20944/preprints202105.0252.v1

Fogang's [1] model consists of realizing an opening of the beam at point i and introducing additional points (fictive points) in the opening (Figure 4a,b and Figure 5a,b).

2.1.3.1.1 W–Φ FDM approximation of a uniform beam

Figure 4a,b below shows the additional points (fictive points ia, id) introduced in the opening. The unknowns at any point are the deflection and the rotation of the cross section.

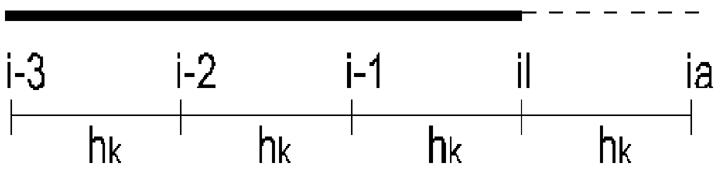

(4a)

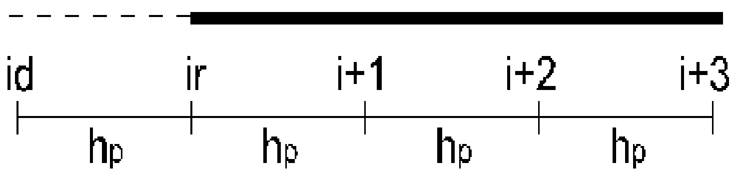

(4b)

Figure 4. Opening of the beam and introduction of additional points on the left side (a) and the right side (b).

The governing equations (Equations (10a-b)) are applied at any point of the beam: …i-1, il, ir, i+1 …

Thus, the governing equations at position il are as follows:

$$\beta_{Vk}W_{i-1}-\left(2\beta_{Vk}+\alpha_r\beta_{lk}^2\frac{k_i l^4}{EI_r}\right)W_{il}+\beta_{Vk}W_{ia}+\frac{\beta_{Vk}}{2}h_k\Phi_{i-1}-\frac{\beta_{Vk}}{2}h_k\Phi_{ia}=-\frac{\alpha_r}{\beta_{lk}^2}q_{il}h_k^4 \tag{19a}$$

$$-\frac{\beta_{Vk}\beta_{lk}^2}{2\alpha_r}W_{i-1}+\frac{\beta_{Vk}\beta_{lk}^2}{2\alpha_r}W_{ia}+\beta_{Mk}h_k\Phi_{i-1}-\left(2\beta_{Mk}+\frac{\beta_{Vk}\beta_{lk}^2}{\alpha_r}\right)h_k\Phi_{il}+\beta_{Mk}h_k\Phi_{ia}=0 \tag{19b}$$

The governing equations at position ir are similarly formulated. The continuity equations express the continuity of the deflection and the rotation of the cross section, and the bending moment and shear force equilibrium (Equations (11a-b)):

$$w_{il}=w_{ir}\rightarrow W_{il}=W_{ir} \tag{20a}$$

$$\varphi_{il}=\varphi_{ir}\rightarrow \Phi_{il}=\Phi_{ir} \tag{20b}$$

$$M_{il}-M_{ir}=M^*\rightarrow \beta_{Mk}\frac{\Phi_{i-1}-\Phi_{ia}}{2h_k}-\beta_{Mp}\frac{\Phi_{id}-\Phi_{i+1}}{2h_p}=M^* \tag{20c}$$

$$V_{il}-V_{ir}=P$$

$$\rightarrow\frac{\beta_{Vk}\beta_{lk}^2}{\alpha_r h_k^3}\left(-\frac{W_{i-1}}{2}+\frac{W_{ia}}{2}-h_k\Phi_{il}\right)-\frac{\beta_{Vp}\beta_{lp}^2}{\alpha_r h_p^3}\left(-\frac{W_{id}}{2}+\frac{W_{i+1}}{2}-h_p\Phi_{ir}\right)=P \tag{20d}$$

Preprints (www.preprints.org) | NOT PEER-REVIEWED | Posted: 11 May 2021 doi:10.20944/preprints202105.0252.v1

An adjustment of the continuity equations is made in the case of a hinge (no continuity of the rotation of the cross section; $M_{il} = M_{ir} = 0$), a support ($W_{il} = W_{ir} = 0$, no Equation (20d)), or a spring.
At the beam's ends, additional points are introduced (Figure 4a,b), so governing equations are applied at the beam's ends, as well as boundary conditions.

2.1.3.1.2 W FDM approximation of a uniform beam

Figure 5a,b below shows the additional points (fictive points ia, ib, ic, id) introduced in the opening. The unknown at any point is the deflection.

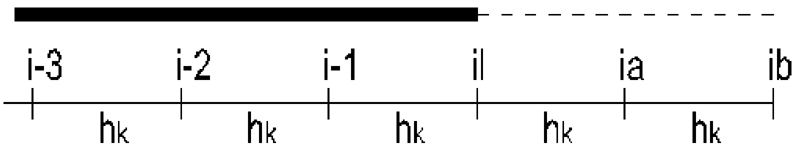

(5a)

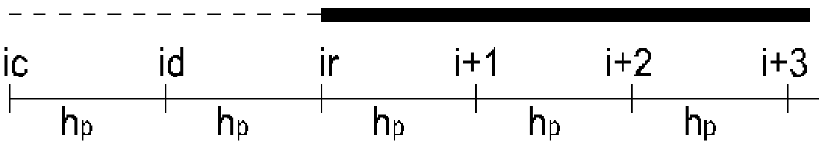

(5b)

Figure 5. Opening of the beam and introduction of additional points on the left side (a) and the right side (b).

The governing equation (Equation (12a)) is applied at any point of the beam: … i-2, i-1, il, ir, i+1, i+2… Thus, the governing equation (Equation (12a)) at position il is formulated by adopting for i, i+1, and i+2 the values of il, ia, and ib, respectively. Similarly, the governing equation at position ir is formulated by adopting for i, i-1, and i-2 the values of ir, id, and ic, respectively.
The continuity equations can be expressed using Equations (13a-c), as follows:

$$w_{il} = w_{ir} \rightarrow W_{il} = W_{ir} \tag{21a}$$

$$\varphi_{il} = \varphi_{ir} \rightarrow EI_r \times \varphi_{il} = EI_r \times \varphi_{ir} \tag{21b}$$

$$M_{il} - M_{ir} = M^* \tag{21c}$$

$$V_{il} - V_{ir} = P \tag{21d}$$

In the equations above, φ_{il}, M_{il}, and V_{il} are formulated by adopting for i, i+1, and i+2 the values of il, ia, and ib, respectively. Similarly, φ_{ir}, M_{ir}, and V_{ir} are formulated by adopting for i, i-1, and i-2 the values of ir, id, and ic, respectively.

2.1.3.1.3 M–W FDM approximation of a uniform beam

The additional points of Figure 4a,b are introduced. The unknowns at any point are the deflection and the bending moment. The governing equations (Equations (13d-e)) are applied at any point of the beam: … i-1, il, ir, i+1 … The

Preprints (www.preprints.org) | NOT PEER-REVIEWED | Posted: 11 May 2021 doi:10.20944/preprints202105.0252.v1

continuity equations can be expressed using Equations (21a-d); the shear force and the rotation of the cross section are calculated using Equations (13f) and (13g), respectively.

2.1.3.1.4 Mixed FDM approximation of a uniform beam

Different approximations (W–Φ, W, and M–W) can be considered on either side of the point of discontinuity. The continuity equations are then formulated with the corresponding formulas.

2.1.3.2 Tapered beam within segments

As described in Section 2.1.3.1, an opening of the beam is realized at point i and additional points (fictive points ia, id) are introduced in the opening (Figure 4a,b).

2.1.3.2.1 W–Φ FDM approximation of a tapered beam

The governing equations (Equations (15a-b)) are applied at any point of the beam: … i-1, il, ir, i+1 … The continuity equations can be expressed through an adjustment of Equations (20a-d), as follows:

$$\beta_{Mk} = \beta_{Mil} \qquad \beta_{Mp} = \beta_{Mir} \qquad \beta_{Vk} = \beta_{Vil} \qquad \beta_{Vp} = \beta_{Vir} \tag{22}$$

2.1.3.2.2 M–W FDM approximation of a tapered beam

The governing equations (Equations (13d) and (16)) are applied at any point of the beam: … i-1, il, ir, i+1 … The continuity equations can be expressed using Equations (21a-d), while the shear force and the rotation of the cross section are calculated using Equations (13f) and (13g), respectively. However, β_{Vk} is replaced by β_{Vi} in Equation (13g).

2.1.3.2.3 Mixed FDM approximation of a tapered beam

Similar to the uniform beam, different approximations (W–Φ, M–W) can be considered on either side of the point of discontinuity. The continuity equations are then formulated with the corresponding formulas.

2.1.3.3 Non-uniform grid

The grid may be such that every node has a non-constant distance from another (Figure 6).

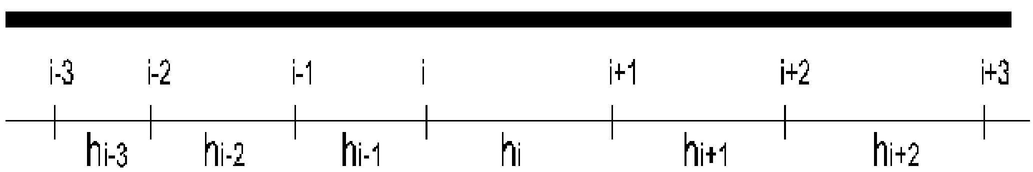

Figure 6. Beam with a non-uniform grid.

In this paper, the Lagrange interpolation polynomial (Equation (7b)) was used for FDM formulations. The resulting equations were complicated, so, the non-uniform grid was not further analyzed. In fact, it should not be analyzed as a discontinuity position.

2.1.4 First-order element stiffness matrix of a tapered beam

2.1.4.1 4×4 element stiffness matrix

The sign convention for bending moments, shear forces, displacements, and rotations of the cross section adopted to determine the element stiffness matrix in local coordinates is illustrated in Figure 7.

Figure 7. Sign convention for moments, shear forces, displacements, and rotations for the stiffness matrix.

Let us define the following vectors:

$$\overrightarrow{S_{red}} = [V_i ; M_i ; V_k ; M_k]^T \quad (23a)$$

$$\overrightarrow{V_{red}} = [w_i ; \varphi_i ; w_k ; \varphi_k]^T \quad (23b)$$

The 4×4 element stiffness matrix in local coordinates of the tapered beam is denoted by K_{44}.

The vectors defined are related together with the element stiffness matrix K_{44}, as follows:

$$\overrightarrow{S_{red}} = K_{44} \times \overrightarrow{V_{red}} \quad (24)$$

Let us divide the beam in n parts of equal length h ($l = nh_k$), as shown in Figure 8.

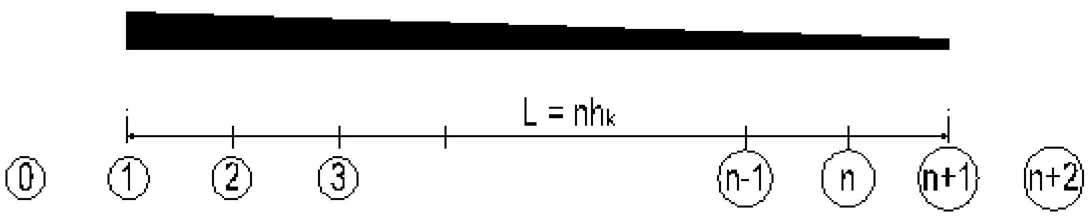

Figure 8. Finite difference method (FDM) discretization for 4x4 element stiffness matrix.

2.1.4.1.1 W–Φ FDM approximation

Equations (15a-b) with $q_i = 0$ and $k_i = 0$ are applied at any point on the grid (nodes 1, 2, …n+1 of Figure 8).

Preprints (www.preprints.org) | NOT PEER-REVIEWED | Posted: 11 May 2021 doi:10.20944/preprints202105.0252.v1

Considering the sign convention adopted for bending moments and shear forces in general (Figure 1) and in the element stiffness matrix (Figure 7), the following static compatibility boundary conditions can be set in combination with Equations (11a-b):

$$V_i = -V_1 = -\frac{\beta_{V1}\beta_{lk}^2}{\alpha_r h_k^{\ 3}}\left(-\frac{W_0}{2}+\frac{W_2}{2}-h_k\Phi_1\right) \rightarrow \frac{\alpha_r h_k^{\ 3}}{\beta_{V1}\beta_{lk}^2}V_i - \frac{W_0}{2}+\frac{W_2}{2}-h_k\Phi_1 = 0 \quad (25a)$$

$$M_i = M_1 = \beta_{M1}\frac{\Phi_0-\Phi_2}{2h_k} \rightarrow \frac{2h_k^{\ 2}}{\beta_{M1}}M_i - h_k\Phi_0 + h_k\Phi_2 = 0 \quad (25b)$$

$$V_k = V_{n+1} = \frac{\beta_{Vn+1}\beta_{lk}^2}{\alpha_r h_k^{\ 3}}\left(-\frac{W_n}{2}+\frac{W_{n+2}}{2}-h_k\Phi_{n+1}\right) \rightarrow \frac{\alpha_r h_k^{\ 3}}{\beta_{Vn+1}\beta_{lk}^2}V_k + \frac{W_n}{2}-\frac{W_{n+2}}{2}+h_k\Phi_{n+1n} = 0 \quad (25c)$$

$$M_k = -M_{n+1} = -\beta_{Mn+1}\frac{\Phi_n-\Phi_{n+2}}{2h_k} \rightarrow \frac{2h_k^{\ 2}}{\beta_{Mn+1}}M_k + h_k\Phi_n - h_k\Phi_{n+2} = 0 \quad (25d)$$

Considering the sign convention adopted for displacements and rotations of cross sections in general (Figure 1) and in the element stiffness matrix (Figure 7), the following geometric compatibility boundary conditions can be set:

$$w_1 = w_i \rightarrow W_1 = EI_r \times w_i \quad (26a) \qquad w_{n+1} = w_k \rightarrow W_{n+1} = EI_r \times w_k \quad (26c)$$

$$\varphi_1 = \varphi_i \rightarrow \Phi_1 = EI_r \times \varphi_i \quad (26b) \qquad \varphi_{n+1} = \varphi_k \rightarrow \Phi_{n+1} = EI_r \times \varphi_k \quad (26d)$$

The number of equations is 2(n+1) + 4 + 4 = **2n + 10**. The number of unknowns is 2(n+3) + 4 = **2n + 10**, especially 2(n+3) unknowns (W; Φ) at points on the beam and additional points at the beam's ends, and four efforts at the beam's ends (Vi; Mi; Vk; Mk). Let us define the following vector

$$\vec{S}_1 = \left[W_0;\Phi_0;W_1;\Phi_1 .... W_{n+2};\Phi_{n+2}\right]^T \quad (27)$$

The combination of Equations (15a-b) applied at any point on the grid, Equations (25a–d), and Equations (26a–d) can be expressed with matrix notation as follows, the geometric compatibility boundary conditions (Equations (26a–d)) being at the bottom:

$$T \times \begin{bmatrix} \vec{S}_1 \\ \vec{S}_{red} \end{bmatrix} = \begin{bmatrix} \vec{0} \\ EI_r \times \vec{V}_{red} \end{bmatrix} \rightarrow \begin{bmatrix} \vec{S}_1 \\ \vec{S}_{red} \end{bmatrix} = T^{-1} \times \begin{bmatrix} \vec{0} \\ EI_r \times \vec{V}_{red} \end{bmatrix} \quad (28)$$

The matrix **T** has 2n+10 rows and 2n+10 columns. The zero vector above has 2n+6 rows.

$$T^{-1} = \begin{bmatrix} T_{aa} & T_{ab} \\ T_{ba} & T_{bb} \end{bmatrix} \quad (29)$$

The matrix T_{aa} has 2n+6 rows and 2n+6 columns, the matrix T_{ab} has 2n+6 rows and 4 columns, the matrix T_{ba} has 4 rows and 2n+6 columns, and the matrix T_{bb} has 4 rows and 4 columns.

The combination of Equations (24), (28), and (29) yields the element stiffness matrix of the beam.

$$K_{44} = EI_r \times T_{bb} \tag{30a}$$

A general matrix formulation of K_{44} is as follows:

$$K_{44} = EI_r \times \begin{bmatrix} 0 & I \end{bmatrix} \times T^{-1} \times \begin{bmatrix} 0^T \\ I \end{bmatrix} \tag{30b}$$

In Equation (30b), 0 is a zero matrix with 4 rows and 2n+6 columns, and I is the 4×4 identity matrix.

2.1.4.1.2 M–W FDM approximation

Equations (13d) and (16) with $q_i = 0$ and $k_i = 0$ are applied at any point on the grid (nodes 1, 2, …n+1 of Figure 8).

The static compatibility boundary conditions in combination with Equations (1b) and (8b) can be expressed as follows:

$$V_i = -V_1 = -\left.\frac{dM(x)}{dx}\right|_1 = -\frac{M_2 - M_0}{2h_k} \rightarrow 2h_k V_i + M_2 - M_0 = 0 \tag{31a}$$

$$M_i = M_1 \rightarrow M_i - M_1 = 0 \tag{31b}$$

$$V_k = V_{n+1} = \left.\frac{dM(x)}{dx}\right|_{n+1} = \frac{M_{n+2} - M_n}{2h_k} \rightarrow 2h_k V_k - M_{n+2} + M_n = 0 \tag{31c}$$

$$M_k = -M_{n+1} \rightarrow M_k + M_{n+1} = 0 \tag{31d}$$

The geometric compatibility boundary conditions in combination with Equations (16d) are

$$w_1 = w_i \rightarrow W_1 = EI_r \times w_i \tag{31e}$$

$$\varphi_1 = \varphi_i \rightarrow EI_r \times \varphi_1 = \frac{W_2 - W_0}{2h_k} - \frac{\alpha_r}{2h_k \beta_{V1} \beta_{lk}^2}\left(h_k{}^2 M_2 - h_k{}^2 M_0\right) = EI_r \times \varphi_i \tag{31f}$$

$$w_{n+1} = w_k \rightarrow W_{n+1} = EI_r \times w_k \tag{31g}$$

$$\varphi_{n+1} = \varphi_k \rightarrow EI_r \times \varphi_{n+1} = \frac{W_{n+2} - W_n}{2h_k} - \frac{\alpha_r}{2h_k \beta_{Vn+1} \beta_{lk}^2}\left(h_k{}^2 M_{n+2} - h_k{}^2 M_n\right) = EI_r \times \varphi_k \tag{31h}$$

The analysis continues similarly to Section 2.1.4.1.1 (Equations (27)-(30b)).

Preprints (www.preprints.org) | NOT PEER-REVIEWED | Posted: 11 May 2021 doi:10.20944/preprints202105.0252.v1

2.1.4.2 3×3 element stiffness matrix

Assuming the presence of a hinge at the right end, the sign convention for bending moments, shear forces, displacements, and rotations of the cross section is illustrated in Figure 9.

Figure 9. Sign convention for moments, shear forces, displacements, and rotations for the stiffness matrix.

The 3×3 element stiffness matrix in local coordinates of the tapered beam is denoted by K_{33}.

The vectors of Equations (23a-b) and (24) become

$$\overrightarrow{S_{red}} = [V_i; M_i; V_k]^T \tag{32a}$$

$$\overrightarrow{V_{red}} = [w_i; \varphi_i; w_k]^T \tag{32b}$$

$$\overrightarrow{S_{red}} = K_{33} \times \overrightarrow{V_{red}} \tag{32c}$$

The matrix K_{33} can be formulated with the values of the matrix K_{44} (see Equations (30a-b)).

$$K_{44} = \begin{bmatrix} K_{aa} & K_{ab} \\ K_{ba} & K_{bb} \end{bmatrix} \tag{33}$$

The matrix K_{44} has 4 rows and 4 columns, the matrix K_{aa} has 3 rows and 3 columns, the matrix K_{ab} has 3 rows and 1 column, the matrix K_{ba} has 1 row and 3 columns, and the matrix K_{bb} has 1 row and 1 column (a single value).

The combination of Equation (24) with the presence of a hinge at position k ($M_k = 0$) and Equation (32c) yields the matrix K_{33}, as follows:

$$K_{33} = K_{aa} - K_{ab} \times \frac{1}{K_{bb}} \times K_{ba} \tag{34}$$

2.2 Second-order analysis

The equation of static equilibrium can be expressed as follows:

$$\frac{dT(x)}{dx} - k(x)w(x) = -q(x) \tag{35a}$$

$$\frac{dM(x)}{dx} - T(x) + N(x)\frac{dw(x)}{dx} = 0 \tag{35b}$$

Preprints (www.preprints.org) | NOT PEER-REVIEWED | Posted: 11 May 2021 doi:10.20944/preprints202105.0252.v1

The axial force (positive in tension) is denoted by N(x) and the transverse force by T(x). Let us consider an external distributed axial load n(x) positive along the + x axis

$$n(x) = -\frac{dN(x)}{dx} \tag{36}$$

The transverse force T(x) is related to the shear force V(x), as follows:

$$T(x) = V(x) + N(x)\frac{dw(x)}{dx} \tag{37}$$

2.2.1 Second-order analysis of a uniform beam within segments

The grid spacing h_k, the reference flexural rigidity EI_r, the reference shear stiffness κGA_r, and the parameters β_{lk}, β_{Mk}, β_{Vk}, and α_r are as defined in previous sections.

2.2.1.1 W–Φ FDM approximation of a uniform beam

Substituting Equations (4), (36), and (37) into Equation (35a) yields

$$\kappa GA \times \left(\frac{d^2 w(x)}{dx^2} - \frac{d\varphi(x)}{dx} \right) + N(x)\frac{d^2 w(x)}{dx^2} - n(x)\frac{dw(x)}{dx} - kw(x) = -q(x) \tag{38}$$

Substituting Equation (37) into Equation (35b) yields Equation (1b). Substituting Equations (3) and (4) into Equation (1b) yields Equation (5b).

Substituting Equations (8a-b) and (9a-f) into Equations (5b) and (38) yields Equation (10b) and the following equation:

$$\left(\frac{\beta_{Vk}\beta_{lk}^2}{\alpha_r} + \frac{N_i h_k^{\ 2}}{EI_r} + \frac{n_i h_k^{\ 3}}{2EI_r} \right) W_{i-1} - \left(2\frac{\beta_{Vk}\beta_{lk}^2}{\alpha_r} + \frac{2N_i h_k^{\ 2}}{EI_r} + \beta_{lk}^4 \frac{k_i l^4}{EI_r} \right) W_i + \left(\frac{\beta_{Vk}\beta_{lk}^2}{\alpha_r} + \frac{N_i h_k^{\ 2}}{EI_r} - \frac{n_i h_k^{\ 3}}{2EI_r} \right) W_{i+1}$$
$$+ \frac{\beta_{Vk}\beta_{lk}^2}{2\alpha_r} h_k \Phi_{i-1} - \frac{\beta_{Vk}\beta_{lk}^2}{2\alpha_r} h_k \Phi_{i+1} = -q_i h_k^{\ 4} \tag{39}$$

Equations (10b) and (39) are applied at any point on the grid. At point i, the external distributed axial load n_i is calculated similarly to Equations (17a–c). Applying Equations (8b) and (11b) into Equation (37) yields the FDM formulation of the transverse force:

$$T_i = -\frac{1}{h_k^{\ 3}} \left(\frac{\beta_{Vk}\beta_{lk}^2}{2\alpha_r} + \frac{N_i h_k^{\ 2}}{2EI_r} \right) W_{i-1} + \frac{1}{h_k^{\ 3}} \left(\frac{\beta_{Vk}\beta_{lk}^2}{2\alpha_r} + \frac{N_i h_k^{\ 2}}{2EI_r} \right) W_{i+1} - \frac{1}{h_k^{\ 3}} \frac{\beta_{Vk}\beta_{lk}^2}{\alpha_r} h_k \Phi_i \tag{40}$$

The bending moment is calculated using Equation (11a). The analysis at positions of discontinuity is conducted similarly to the first-order analysis; however, the shear force is replaced by the transverse force.

Preprints (www.preprints.org) | NOT PEER-REVIEWED | Posted: 11 May 2021 doi:10.20944/preprints202105.0252.v1

2.2.1.2 W FDM approximation of a uniform beam

It is assumed here that the axial force and stiffness of the Winkler foundation are constant along the beam. Substituting Equations (2), (36), and (37) into Equation (35a) yields

$$\frac{d^2M(x)}{dx^2}+N\frac{d^2w(x)}{dx^2}-kw(x)=-q(x) \tag{41}$$

Equation (6c) also holds in second-order analysis.

Differentiating Equations (41) and (6c) twice with respect to x and combining the results with Equation (41) yields

$$(1+\frac{N}{\kappa GA})\frac{d^4w(x)}{dx^4}-(\frac{N}{EI}+\frac{k}{\kappa GA})\frac{d^2w(x)}{dx^2}+\frac{k}{EI}w(x)=\frac{q(x)}{EI}-\frac{1}{\kappa GA}\frac{d^2q(x)}{dx^2} \tag{42a}$$

Combining Equations (41) and (6c) yields

$$\frac{M(x)}{EI}=-(1+\frac{N}{\kappa GA})\frac{d^2w(x)}{dx^2}+\frac{k}{\kappa GA}w(x)-\frac{q(x)}{\kappa GA} \tag{42b}$$

The parameter k_w of the Winkler foundation is defined in Equation (12b). Let us introduce the parameter k_N, as follows:

$$N=k_N\frac{EI_r}{l^2} \tag{42c}$$

Substituting Equations (8c), (8e), (9a-e), and (42c) into the governing Equation (42a) yields

$$(1+\frac{k_N\alpha_r}{\beta_{Vk}})\left(W_{i-2}-4W_{i-1}+6W_i-4W_{i+1}+W_{i+2}\right)-\beta_{lk}^2(\frac{k_N}{\beta_{Mk}}+\frac{k_W\alpha_r}{\beta_{Vk}})\frac{-W_{i-2}+16W_{i-1}-30W_i+16W_{i+1}-W_{i+2}}{12}$$
$$+\frac{k_W\beta_{lk}^4}{\beta_{Mk}}W_i = \frac{q_ih^4}{\beta_{Mk}}-\frac{\alpha_r}{\beta_{Vk}\beta_{lk}^2}h_k^6\left.\frac{d^2q(x)}{dx^2}\right|_i \tag{43a}$$

The bending moments, the transverse forces, and the rotations of the cross sections are determined using Equations (42b) and (8e), Equations (37), (1b), (42b), (8d), and (8f), and Equations (4), (42b), (1b), (8d), and (8f), respectively.

$$M_i=-\beta_{Mk}(1+\frac{k_N\alpha_r}{\beta_{Vk}})\frac{-W_{i-2}+16W_{i-1}-30W_i+16W_{i+1}-W_{i+2}}{12h_k^2}$$
$$+\frac{k_W\beta_{Mk}\alpha_r\beta_{lk}^2}{\beta_{Vk}}\frac{W_i}{h_k^2}-\frac{\beta_{Mk}\alpha_r}{\beta_{Vk}}l^2q_i \tag{43b}$$

$$T_i=-\beta_{Mk}(1+\frac{k_N\alpha_r}{\beta_{Vk}})\frac{-W_{i-2}+2W_{i-1}-2W_{i+1}+W_{i+2}}{2h_k^3}$$
$$+\beta_{lk}^2\left(\frac{k_W\beta_{Mk}\alpha_r}{\beta_{Vk}}+k_N\right)\frac{W_{i-2}-8W_{i-1}+8W_{i+1}-W_{i+2}}{12h_k^3}-\frac{\beta_{Mk}\alpha_r}{\beta_{Vk}}l^2\left.\frac{dq(x)}{dx}\right|_i \tag{43c}$$

Preprints (www.preprints.org) | NOT PEER-REVIEWED | Posted: 11 May 2021 doi:10.20944/preprints202105.0252.v1

$$EI_r\varphi_i = \frac{\beta_{Mk}\alpha_r}{\beta_{Vk}\beta_{lk}^2}(1+\frac{k_N\alpha_r}{\beta_{Vk}})\frac{-W_{i-2}+2W_{i-1}-2W_{i+1}+W_{i+2}}{2h_k}$$
$$+\left(1-\frac{k_W\beta_{Mk}\alpha_r^2}{\beta_{VK}^2}\right)\frac{W_{i-2}-8W_{i-1}+8W_{i+1}-W_{i+2}}{12h_k}+\frac{\beta_{Mk}\alpha_r^2}{\beta_{VK}^2}l^4\frac{dq(x)}{dx}\bigg|_i \quad (43d)$$

2.2.1.3 M–W FDM approximation of a uniform beam

Substituting Equations (2), (36), and (37) into Equation (35a) yields

$$\frac{d^2M(x)}{dx^2}+N(x)\frac{d^2w(x)}{dx^2}-n(x)\frac{dw(x)}{dx}-kw(x)=-q(x) \quad (43e)$$

Substituting Equations (8a-b) and (9d-e) into Equation (43e) yields

$$h_k^{\ 2}M_{i-1}-2h_k^{\ 2}M_i+h_k^{\ 2}M_{i+1}+\left(\frac{N_ih_k^{\ 2}}{EI_r}+\frac{n_ih_k^{\ 3}}{2EI_r}\right)W_{i-1}-\left(\frac{2N_ih_k^{\ 2}}{EI_r}+\beta_{lk}^4\frac{k_il^4}{EI_r}\right)W_i \quad (43f)$$
$$+\left(\frac{N_ih_k^{\ 2}}{EI_r}-\frac{n_ih_k^{\ 3}}{2EI_r}\right)W_{i+1}=-q_ih_k^{\ 4}$$

The governing equations (Equations (43f) and (13e)) are applied at any point on the grid. The rotation of the cross section is calculated using Equations (13g). Applying Equations (37), (1b), and (8b) yields the transverse force, as follows:

$$2h_k^3T_i=h_k^2M_{i+1}-h_k^2M_{i-1}+\frac{N_ih_k^2}{EI_r}(W_{i+1}-W_{i-1}) \quad (43g)$$

2.2.2 Second-order analysis of a tapered beam

2.2.2.1 W–Φ FDM approximation of a tapered beam

Substituting Equations (4), (36), and (37) into Equation (35a) yields

$$\frac{d\kappa GA(x)}{dx}\times\left(\frac{dw(x)}{dx}-\varphi(x)\right)+\kappa GA(x)\times\left(\frac{d^2w(x)}{dx^2}-\frac{d\varphi(x)}{dx}\right) \quad (44a)$$
$$+N(x)\frac{d^2w(x)}{dx^2}-n(x)\frac{dw(x)}{dx}-kw(x)=-q(x)$$

The grid spacing in segment k is h_k. The reference flexural rigidity EI_r, the reference shear stiffness κGA_r, and the parameters α_r,β_{Vi}, and β'_{Vi} (Equations (9c-f) and (14a-d)) are defined. Substituting Equations (8a-b), (9c-f), and (14a-d) into Equation (44a) yields

$$\left(-\frac{\beta'_{Vi}\beta_{lk}^2}{2\alpha_r}+\frac{\beta_{Vi}\beta_{lk}^2}{\alpha_r}+\frac{N_ih_k^{\ 2}}{EI_r}+\frac{n_ih_k^{\ 3}}{2EI_r}\right)W_{i-1}-\left(\frac{2\beta_{Vi}\beta_{lk}^2}{\alpha_r}+\frac{2N_ih_k^{\ 2}}{EI_r}+\beta_{lk}^4\frac{k_il^4}{EI_r}\right)W_i \quad (44b)$$
$$+\left(\frac{\beta'_{Vi}\beta_{lk}^2}{2\alpha_r}+\frac{\beta_{Vi}\beta_{lk}^2}{\alpha_r}+\frac{N_ih_k^{\ 2}}{EI_r}-\frac{n_ih_k^{\ 3}}{2EI_r}\right)W_{i+1}+\frac{\beta_{Vi}\beta_{lk}^2}{2\alpha_r}h_k\Phi_{i-1}-\frac{\beta'_{Vi}\beta_{lk}^2}{\alpha_r}h_k\Phi_i-\frac{\beta_{Vi}\beta_{lk}^2}{2\alpha_r}h_k\Phi_{i+1}=-q_ih_k^4$$

Preprints (www.preprints.org) | NOT PEER-REVIEWED | Posted: 11 May 2021 doi:10.20944/preprints202105.0252.v1

Equations (15b) and (44b) are applied at any point on the grid.

The bending moments and the transverse forces are calculated using Equations (11a) and (40), β_{Mk} and β_{Vk} being replaced by β_{Mi} and β_{Vi}.

2.2.2.2 M–W FDM approximation of a tapered beam

The governing equations (Equations (16) and (43f)) are applied at any point on the grid. The rotations of the cross sections and the transverse forces are calculated using Equations (13g) and (43g), respectively. However, β_{Vk} is replaced by β_{Vi} in Equation (13g).

2.2.3 Second-order element stiffness matrix of a uniform beam

The beam is divided in n parts of equal length h_k, as shown in Figure 10.

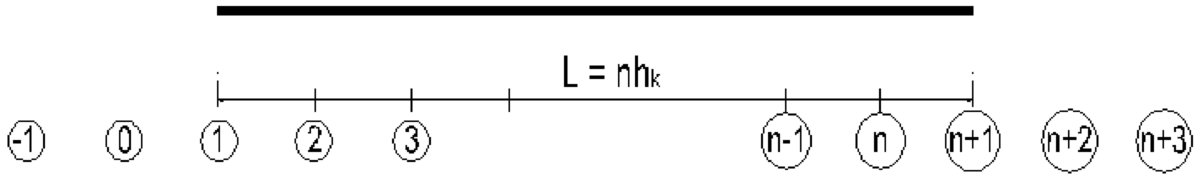

Figure 10. FDM discretization for 4×4 element stiffness matrix.

The sign convention for bending moments, transverse forces, displacements, and rotations of the cross sections adopted to determine the element stiffness matrix in local coordinates is illustrated in Figure 7, the shear forces V_i and V_k being replaced by the transverse forces T_i and T_k.

The W FDM approximation is applied here. The W–Φ FDM and M–W FDM approximations can also be considered with appropriate formulas developed in previous sections.

Equation (43a) with $q_i = 0$ and $k_W = 0$ is applied at any point on the grid (nodes 1, 2, …n+1 of Figure 10).

The static compatibility boundary conditions are applied using Equations (43b-c). The geometric compatibility boundary conditions are applied similarly to Equations (26a-d), the rotation of the cross section being formulated with Equation (43d). The analysis continues similarly to Section 2.1.4.1.1 (Equations (27)-(30b)).

2.2.4 Second-order element stiffness matrix of a tapered beam

The M–W FDM approximation is applied here. The W–Φ FDM approximation can also be applied with appropriate formulas developed previously. The sign convention for bending moments, transverse forces, displacements, and rotations

Preprints (www.preprints.org) | NOT PEER-REVIEWED | Posted: 11 May 2021 doi:10.20944/preprints202105.0252.v1

of the cross sections adopted to determine the element stiffness matrix in local coordinates is illustrated in Figure 7, the shear forces V_i and V_k being replaced by the transverse forces T_i and T_k.

Equations (16) and (43f) with qi = 0 and ki = 0 are applied at any point on the grid (nodes 1, 2, …n+1 of Figure 8). The static compatibility boundary conditions are expressed similarly to Equations (31a–d); however, the shear forces are replaced by the transverse forces (Equation (43g)). The geometric compatibility boundary conditions are the same as in Section 2.1.4.1.2 (Equations (31e-h)). The analysis continues similarly to Section 2.1.4.1.1 (Equations (27)-(30b)).

2.3 Vibration analysis of the Timoshenko beam

2.3.1 Free vibration analysis

The focus here is to determine the eigenfrequencies of the beam. A second-order analysis is conducted; and the first-order analysis can easily be deduced. The equations of dynamic equilibrium on an infinitesimal beam element are as follows:

$$\frac{\partial T^*(x,t)}{\partial x} - k(x)w^*(x,t) = \rho A(x)\frac{\partial^2 w^*(x,t)}{\partial t^2} \tag{45}$$

$$\frac{\partial M^*(x,t)}{\partial x} + N(x)\frac{\partial w^*(x,t)}{\partial x} - T^*(x,t) = -\rho I(x)\frac{\partial^2 \varphi^*(x,t)}{\partial t^2} \tag{46}$$

where ρ is the beam's mass per unit volume, A(x) is the cross-sectional area, N(x) is the axial force (positive in tension), and k(x) is the stiffness of the elastic Winkler foundation.

A harmonic vibration being assumed, $T^*(x,t)$, $M^*(x,t)$, $w^*(x,t)$, and $\varphi^*(x,t)$ can be expressed as follows ($S^*(x,t)$ representing $T^*(x,t)$, $M^*(x,t)$, $w^*(x,t)$, and $\varphi^*(x,t)$):

$$S^*(x,t) = S(x)\times\sin(\omega t + \theta) \tag{47}$$

where ω is the circular frequency of the beam. Substituting Equation (47) into Equations (45) and (46) yields

$$\frac{dT(x)}{dx} - k(x)w(x) + \rho A(x)\omega^2 w(x) = 0 \tag{48a}$$

$$\frac{dM(x)}{dx} + N(x)\frac{dw(x)}{dx} - T(x) - \rho I(x)\omega^2\varphi(x) = 0 \tag{48b}$$

Substituting Equations (36) and (37) into Equations (48a-b) yields

$$\frac{dV(x)}{dx} + N(x)\frac{d^2w(x)}{dx^2} - n(x)\frac{dw(x)}{dx} - k(x)w(x) + \rho A(x)\omega^2 w(x) = 0 \tag{49a}$$

$$\frac{dM(x)}{dx} - V(x) - \rho I(x)\omega^2\varphi(x) = 0 \tag{49b}$$

2.3.1.1 Uniform beam within segments

2.3.1.1.1 W–Φ FDM approximation of a uniform beam

We defined (Equations (9a-c)) a reference flexural stiffness EI_r, a reference shear stiffness κGA_r, parameters β_{Mk}, β_{Vk}, and α_r. A reference cross-sectional area A_r and a reference length l_r are also defined and are related to the cross-sectional area A_k and the grid spacing h_k in the segment, as follows:

$$A_k = \beta_{AK} A_r \tag{50a}$$

$$h_k = \beta_{lk} l_r \tag{50b}$$

The parameter α_r (Equation (9c)) is defined with l_r instead of l. Substituting Equations (3) and (4) into Equations (49a-b) and combining the results with Equations (8a-b) yields the following FDM formulations:

$$\left(\frac{\beta_{Vk}\beta_{lk}^2}{\alpha_r}+\frac{N_i h_k{}^2}{EI_r}+\frac{n_i h_k{}^3}{2EI_r}\right)W_{i-1}-\left(2\frac{\beta_{Vk}\beta_{lk}^2}{\alpha_r}+\frac{2N_i h_k{}^2}{EI_r}+\beta_{lk}^4\frac{k_i l_r{}^4}{EI_r}-\frac{\beta_{Ak}\beta_{lk}^4\rho A_r\omega^2 l_r{}^4}{EI_r}\right)W_i$$
$$+\left(\frac{\beta_{Vk}\beta_{lk}^2}{\alpha_r}+\frac{N_i h_k{}^2}{EI_r}-\frac{n_i h_k{}^3}{2EI_r}\right)W_{i+1}+\frac{\beta_{Vk}\beta_{lk}^2}{2\alpha_r}h_k\Phi_{i-1}-\frac{\beta_{Vk}\beta_{lk}^2}{2\alpha_r}h_k\Phi_{i+1}=0 \tag{51a}$$

$$-\frac{\beta_{Vk}\beta_{lk}^2}{2\alpha_r}W_{i-1}+\frac{\beta_{Vk}\beta_{lk}^2}{2\alpha_r}W_{i+1}+\beta_{Mk}h_k\Phi_{i-1}-\left(2\beta_{Mk}+\frac{\beta_{Vk}\beta_{lk}^2}{\alpha_r}-\frac{\rho I_k\omega^2 h_k{}^2}{EI_r}\right)h_k\Phi_i+\beta_{Mk}h_k\Phi_{i+1}=0 \tag{51b}$$

The reference coefficient of rotary inertia k_{RIr} and the vibration frequency ω are defined as follows

$$k_{RIr}=\frac{I_r}{A_r l_r{}^2} \tag{52a}$$

$$\omega=\lambda\times\sqrt{\frac{EI_r}{\rho A_r l_r{}^4}} \tag{52b}$$

Substituting Equations (52a-b) into Equations (51a-b) yields

$$\left(\frac{\beta_{Vk}\beta_{lk}^2}{\alpha_r}+\frac{N_i h_k{}^2}{EI_r}+\frac{n_i h_k{}^3}{2EI_r}\right)W_{i-1}-\left(\frac{2\beta_{Vk}\beta_{lk}^2}{\alpha_r}+\frac{2N_i h_k{}^2}{EI_r}+\beta_{lk}^4\frac{k_i l_r{}^4}{EI_r}-\beta_{Ak}\beta_{lk}^4\lambda^2\right)W_i$$
$$+\left(\frac{\beta_{Vk}\beta_{lk}^2}{\alpha_r}+\frac{N_i h_k{}^2}{EI_r}-\frac{n_i h_k{}^3}{2EI_r}\right)W_{i+1}+\frac{\beta_{Vk}\beta_{lk}^2}{2\alpha_r}h_k\Phi_{i-1}-\frac{\beta_{Vk}\beta_{lk}^2}{2\alpha_r}h_k\Phi_{i+1}=0 \tag{53a}$$

$$-\frac{\beta_{Vk}\beta_{lk}^2}{2\alpha_r}W_{i-1}+\frac{\beta_{Vk}\beta_{lk}^2}{2\alpha_r}W_{i+1}+\beta_{Mk}h_k\Phi_{i-1}-\left(2\beta_{Mk}+\frac{\beta_{Vk}\beta_{lk}^2}{\alpha_r}-k_{RIr}\beta_{Mk}\beta_{lk}^2\lambda^2\right)h_k\Phi_i$$
$$+\beta_{Mk}h_k\Phi_{i+1}=0 \tag{53b}$$

Preprints (www.preprints.org) | NOT PEER-REVIEWED | Posted: 11 May 2021 doi:10.20944/preprints202105.0252.v1

Equations (53a-b) are applied at any point on the grid. The bending moments and transverse forces are determined using Equations (11a) and (40), respectively.

For the special case of a uniform beam without an axial force or a Winkler foundation, Equations (53a-b) become

$$W_{i-1}-\left(2-\alpha_r\beta_{lk}^2\lambda^2\right)W_i+W_{i+1}+\frac{1}{2}h_k\Phi_{i-1}-\frac{1}{2}h_k\Phi_{i+1}=0 \tag{54a}$$

$$-\frac{\beta_{lk}^2}{2\alpha_r}W_{i-1}+\frac{\beta_{lk}^2}{2\alpha_r}W_{i+1}+h_k\Phi_{i-1}-\left(2+\frac{\beta_{lk}^2}{\alpha_r}-k_{RIr}\beta_{lk}^2\lambda^2\right)h_k\Phi_i+h_k\Phi_{i+1}=0 \tag{54b}$$

Effect of a concentrated mass, or a spring

The dynamic behavior of a beam carrying a concentrated mass or having a spring was analyzed, as shown in Figure 11.

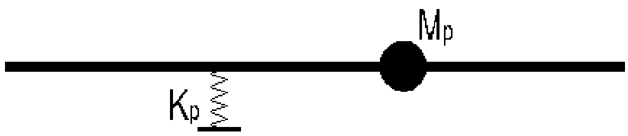

Figure 11. Vibration of beam having a concentrated mass and a spring.

The stiffness of the spring is K_p, and the concentrated mass is M_p.

$$K_p=k_p\times EI_r/l_r^3 \tag{55a}$$

$$M_p=m_p\times\rho A_r l_r \tag{55b}$$

The continuity equations for deflections, rotations of the cross sections, and bending moments are defined in Equations (20a), (20b), and (20c), respectively. Equation (20c) is applied with $M^*=0$. The reference length of the beam is l_r (Equation (50b)).

Applying Equations (9e), (50b), (52b), and (55a-b), the balance of vertical forces in the case of a concentrated mass or a spring yields

$$T_{il}-T_{ir}-\frac{M_p\omega^2}{EI_r}W_{il}=0\rightarrow T_{il}-T_{ir}-\frac{m_p}{l_r^3}\lambda^2W_{il}=0 \quad \text{and} \tag{56a}$$

$$T_{il}-T_{ir}+\frac{K_p}{EI_r}W_{il}=0\rightarrow T_{il}-T_{ir}+\frac{k_p}{l_r^3}W_{il}=0\ , \tag{56b}$$

respectively. The transverse forces T_{il} and T_{ir} are calculated using Equation (40).

Effect of a spring–mass system: The dynamic behavior of a beam carrying a spring–mass system was analyzed, as represented in Figure 12. The deflection of the mass is denoted by w_{iM}.

Preprints (www.preprints.org) | NOT PEER-REVIEWED | Posted: 11 May 2021 doi:10.20944/preprints202105.0252.v1

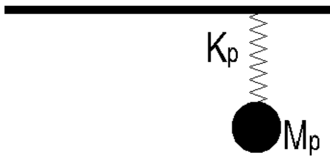

Figure 12. Vibration of a beam carrying a spring–mass system.

Applying Equations (9e), (50b), (52b), and (55a-b), the balance of vertical forces yields

$$T_{il}-T_{ir}-\frac{M_p\omega^2}{EI_r}W_{iM}=0\rightarrow T_{il}-T_{ir}-\frac{m_p}{l_r^{\,3}}\lambda^2W_{iM}=0 \tag{57a}$$

$$\frac{M_p\omega^2}{EI_r}W_{iM}=\frac{K_p}{EI_r}\times(W_{iM}-W_{ir})\rightarrow m_p\lambda^2W_{iM}=k_p(W_{iM}-W_{ir}) \tag{57b}$$

2.3.1.1.2 M–W FDM approximation of a uniform beam

Substituting Equation (49b) into Equation (49a) and combining the result with Equation (3) yields

$$\frac{d^2M(x)}{dx^2}+\frac{\rho\omega^2}{E}M(x)+N(x)\frac{d^2w(x)}{dx^2}-n(x)\frac{dw(x)}{dx}-k(x)w(x)+\rho A\omega^2w(x)=0 \tag{58}$$

Fogang [11] presented the following material law, which combines bending, shear, the curvature, and the natural frequency:

$$\frac{d^2w(x)}{dx^2}+(1-\frac{\rho I\omega^2}{\kappa GA})\times\frac{M(x)}{EI}-\frac{1}{\kappa GA}\times\frac{d^2M(x)}{dx^2}=0 \tag{59a}$$

In [11] the relationship between shear force/rotation of the cross section and bending moment/deflection is presented as follows:

$$\left(1-\frac{\rho I\omega^2}{\kappa GA}\right)\times V(x)=\frac{dM(x)}{dx}-\rho I\omega^2\frac{dw(x)}{dx} \tag{59b}$$

$$\left(\rho I\omega^2-\kappa GA\right)\times\varphi(x)=\frac{dM(x)}{dx}-\kappa GA\frac{dw(x)}{dx} \tag{59c}$$

Substituting Equations (8a-b), (50a-b), and (52a-b) into Equations (58) and (59a) yields

$$h_k^{\,2}M_{i-1}+\left(k_{RIr}\beta_{lk}^2\lambda^2-2\right)h_k^{\,2}M_i+h_k^{\,2}M_{i+1}+\left(\frac{N_ih_k^{\,2}}{EI_r}+\frac{n_ih_k^{\,3}}{2EI_r}\right)W_{i-1}$$
$$-\left(\frac{2N_ih_k^{\,2}}{EI_r}+\beta_{lk}^4\frac{k_il_r^{\,4}}{EI_r}-\beta_{Ak}\beta_{lk}^4\lambda^2\right)W_i+\left(\frac{N_ih_k^{\,2}}{EI_r}-\frac{n_ih_k^{\,3}}{2EI_r}\right)W_{i+1}=0 \tag{60a}$$

$$W_{i-1}-2W_i+W_{i+1}-\frac{\alpha_r}{\beta_{Vk}\beta_{lk}^2}h_k^{\,2}M_{i-1}+\left(\frac{1}{\beta_{Mk}}+\frac{2\alpha_r}{\beta_{Vk}\beta_{lk}^2}-\frac{1}{\beta_{Vk}}k_{RIr}\alpha_r\lambda^2\right)h_k^{\,2}M_i \tag{60b}$$

$$-\frac{\alpha_r}{\beta_{Vk}\beta_{lk}^2}h_k^{\,2}M_{i+1}=0$$

Equations (60a-b) are applied at any point on the grid. The rotation of the cross section and the shear force are calculated substituting Equations (8a-b), (9c), and (52a-b) into Equations (59b-c), as follows:

$$\left(1-\frac{\beta_{Mk}}{\beta_{Vk}}k_{RIr}\alpha_r\lambda^2\right)V_i=\frac{M_{i+1}-M_{i-1}}{2h_k}-\beta_{Mk}\beta_{lk}^2k_{RIr}\lambda^2\frac{W_{i+1}-W_{i-1}}{2h_k^3} \tag{60c}$$

$$\left(\beta_{Mk}\beta_{lk}^2k_{RIr}\lambda^2-\frac{\beta_{Vk}\beta_{lk}^2}{\alpha_r}\right)\frac{EI_r}{h_k^2}\varphi_i=\frac{M_{i+1}-M_{i-1}}{2h_k}-\frac{\beta_{Vk}\beta_{lk}^2}{\alpha_r}\frac{W_{i+1}-W_{i-1}}{2h_k^3} \tag{60d}$$

The transverse force is calculated using Equations (37) and (60c).

The dynamic behavior of a beam carrying a concentrated mass, a spring, or a spring–mass system was analyzed similarly to the previous section (Equations (55a)-(57b)).

2.3.1.2 Tapered beam

The W–Φ FDM approximation was considered here for the vibration analysis of a tapered beam. The M-W FDM approximation led to complicated expressions and was not further analyzed. The beam segment with length l is divided in parts of equal length h_k. The reference values of flexural stiffness, shear stiffness, cross-sectional area, and coefficient of rotary inertia are defined like in previous sections.

Substituting Equations (3) and (4) into Equations (49a-b) and combining the results with Equations (8a-b), (14a-d), (50a-b), and (52a-b) yields the following FDM formulations of the governing equations:

$$\left(-\frac{\beta'_{Vi}\beta_{lk}^2}{2\alpha_r}+\frac{\beta_{Vi}\beta_{lk}^2}{\alpha_r}+\frac{N_ih_k^{\,2}}{EI_r}+\frac{n_ih_k^{\,3}}{2EI_r}\right)W_{i-1}-\left(\frac{2\beta_{Vi}\beta_{lk}^2}{\alpha_r}+\frac{2N_ih_k^{\,2}}{EI_r}+\beta_{lk}^4\frac{k_il_r^4}{EI_r}-\beta_{Ai}\beta_{lk}^4\lambda^2\right)W_i \tag{61a}$$

$$+\left(\frac{\beta'_{Vi}\beta_{lk}^2}{2\alpha_r}+\frac{\beta_{Vi}\beta_{lk}^2}{\alpha_r}+\frac{N_ih_k^{\,2}}{EI_r}-\frac{n_ih_k^{\,3}}{2EI_r}\right)W_{i+1}+\frac{\beta_{Vi}\beta_{lk}^2}{2\alpha_r}h_k\Phi_{i-1}-\frac{\beta'_{Vi}\beta_{lk}^2}{\alpha_r}h_k\Phi_i-\frac{\beta_{Vi}\beta_{lk}^2}{2\alpha_r}h_k\Phi_{i+1}=0$$

Preprints (www.preprints.org) | NOT PEER-REVIEWED | Posted: 11 May 2021 doi:10.20944/preprints202105.0252.v1

$$-\frac{\beta_{Vi}\beta_{lk}^2}{2\alpha_r}W_{i-1}+\frac{\beta_{Vi}\beta_{lk}^2}{2\alpha_r}W_{i+1}+\left(\beta_{Mi}-\frac{\beta_{Mi}^{'}}{2}\right)h_k\Phi_{i-1}-\left(2\beta_{Mi}+\frac{\beta_{Vi}\beta_{lk}^2}{\alpha_r}-k_{RIr}\beta_{Mi}\beta_{lk}^2\lambda^2\right)h_k\Phi_i \tag{61b}$$

$$+\left(\beta_{Mi}+\frac{\beta_{Mi}^{'}}{2}\right)h_k\Phi_{i+1}=0$$

Equations (61a-b) are applied at any point on the grid. The bending moments and transverse forces are determined using Equations (11a) and (40), respectively, β_{Mk} and β_{Vk} being replaced by β_{Mi} and β_{Vi}.

Effect of a concentrated mass, a spring, or a spring–mass system

The dynamic behavior of a beam carrying a concentrated mass, a spring, or a spring–mass system is analyzed similarly to the previous section (Equations (55a)-(57b). The transverse forces T_{il} and T_{ir} are calculated using Equation (40), β_{Vk} being replaced by β_{Vi}.

2.3.2 Direct time integration method

The direct time integration method developed here describes the dynamic response of a beam as a multi-degree-of-freedom system. Viscosity η and external loading p(*x*,*t*) are considered.

2.3.2.1 Uniform beam within segments

The W–Φ FDM approximation was considered for the vibration analysis of the uniform beam. Substituting Equations (3), (4), (36), and (37) into Equations (45) and (46) yields the following governing equation for a uniform beam:

$$\kappa GA\times\left(\frac{\partial^2 w^*(x,t)}{\partial x^2}-\frac{\partial\varphi^*(x,t)}{\partial x}\right)-n(x)\frac{\partial w^*(x,t)}{\partial x}+N(x)\frac{\partial^2 w^*(x,t)}{\partial x^2}$$

$$-k(x)w^*(x,t)-\rho A\frac{\partial^2 w^*(x,t)}{\partial t^2}-\eta\frac{\partial w^*(x,t)}{\partial t}=-p(x,t) \tag{62a}$$

$$EI\frac{\partial^2\varphi^*(x,t)}{\partial x^2}+\kappa GA\times\left(\frac{\partial w^*(x,t)}{\partial x}-\varphi^*(x,t)\right)-\rho I\frac{\partial^2\varphi^*(x,t)}{\partial t^2}=0 \tag{62b}$$

The derivatives with respect to *x* are formulated using Equations (8a-b), while those with respect to *t* (time increment is Δt) are formulated considering a three-point stencil with Equations (63a-c):

$$\left.\frac{\partial w^*(x,t)}{\partial t}\right|_{i,t}=\frac{-w^*_{i,t-\Delta t}+w^*_{i,t+\Delta t}}{2\Delta t}\qquad\left.\frac{\partial^2 w^*(x,t)}{\partial t^2}\right|_{i,t}=\frac{w^*_{i,t-\Delta t}-2w^*_{i,t}+w^*_{i,t+\Delta t}}{\Delta t^2} \tag{63a}$$

 doi:10.20944/preprints202105.0252.v1

At initial time t = 0, a three-point forward difference approximation is applied (Equation (18a)):

$$\left.\frac{\partial^2 w^*}{\partial t^2}\right|_{i,0} = \frac{w^*_{i,0} - 2w^*_{i,\Delta t} + w^*_{i,2\Delta t}}{\Delta t^2} \qquad \left.\frac{\partial w^*}{\partial t}\right|_{i,0} = \frac{-3w^*_{i,0} + 4w^*_{i,\Delta t} - w^*_{i,2\Delta t}}{2\Delta t} \tag{63b}$$

At final time t = T, a three-point backward difference approximation is applied (Equation (18c)):

$$\left.\frac{\partial^2 w^*}{\partial t^2}\right|_{i,T} = \frac{w^*_{i,T-2\Delta t} - 2w^*_{i,T-\Delta t} + w^*_{i,T}}{\Delta t^2} \qquad \left.\frac{\partial w^*}{\partial t}\right|_{i,T} = \frac{w^*_{i,T-2\Delta t} - 4w^*_{i,T-\Delta t} + 3w^*_{i,T}}{2\Delta t} \tag{63c}$$

The governing equations (Equations (62a-b)) can be formulated with the FDM for x = i at time t. The FDM formulations of these equations are applied at any point of the beam at any time t using a five-point stencil. Additional points are introduced to satisfy the boundary and continuity conditions. The boundary conditions are satisfied using a three-point stencil. Thus, beam deflection $w^*(x,t)$ and rotation $\varphi^*(x,t)$ can be determined with the Cartesian model represented in Figure 13. The bending moment $M^*(x,t)$, shear force $V^*(x,t)$, and transverse force $T^*(x,t)$ are calculated using Equations (11a-b) and (37), respectively.

With this model, the assumptions made previously can be verified, namely the separation of variables and the harmonic vibration (Equation (47)).

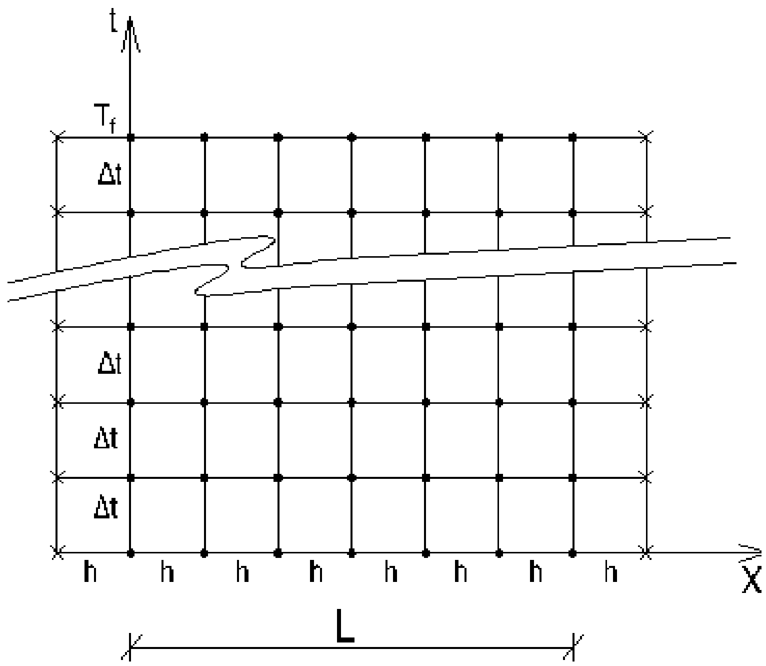

Figure 13. Model for the calculation of time-dependent vibration of a uniform beam.

Preprints (www.preprints.org) | NOT PEER-REVIEWED | Posted: 11 May 2021 doi:10.20944/preprints202105.0252.v1

2.3.2.2 Tapered beam

A similar analysis can be conducted. Thus, Equations (62a-b) become

$$\frac{d\kappa GA(x)}{dx}\left(\frac{\partial w^*(x,t)}{\partial x}-\varphi^*(x,t)\right)+\kappa GA(x)\left(\frac{\partial^2 w^*(x,t)}{\partial x^2}-\frac{\partial \varphi^*(x,t)}{\partial x}\right) \tag{64a}$$

$$-n(x)\frac{\partial w^*(x,t)}{\partial x}+N(x)\frac{\partial^2 w^*(x,t)}{\partial x^2}-k(x)w^*(x,t)-\rho A(x)\frac{\partial^2 w^*(x,t)}{\partial t^2}-\eta\frac{\partial w^*(x,t)}{\partial t}=-p(x,t)$$

$$\frac{dEI(x)}{dx}\frac{\partial \varphi^*(x,t)}{\partial x}+EI(x)\frac{\partial^2 \varphi^*(x,t)}{\partial x^2}+\kappa GA(x)\times\left(\frac{\partial w^*(x,t)}{\partial x}-\varphi^*(x,t)\right)-\rho I(x)\frac{\partial^2 \varphi^*(x,t)}{\partial t^2}=0 \tag{64b}$$

The derivatives with respect to x are formulated using Equations (8a-b), while those with respect to t (time increment is Δt) are formulated considering a three-point stencil with Equations (63a-c).

The FDM formulations of Equations (64a-b) are applied at any point on the beam and at any time t using a five-point stencil. Additional points are introduced to satisfy the boundary and continuity conditions. The boundary conditions are satisfied using a three-point stencil. Thus, beam deflection $w^*(x,t)$ and rotation $\varphi^*(x,t)$ can be determined with the Cartesian model represented in Figure 13. The bending moment $M^*(x,t)$, shear force $V^*(x,t)$, and transverse force $T^*(x,t)$ are calculated using Equations (11a-b) and (37), respectively, β_{Vk} being replaced by β_{Vi} in Equation (11b) and β_{Mk} by β_{Mi} in Equation (11a).

With this model, the assumptions made previously can be verified, namely the separation of variables and the harmonic vibration (Equation (47)).

3 Results and discussion

3.1 First-order analysis

3.1.1 Beam subjected to a uniformly distributed load

In this study, we analyzed a uniform fixed–pinned beam subjected to a uniformly distributed load (Figure 14).

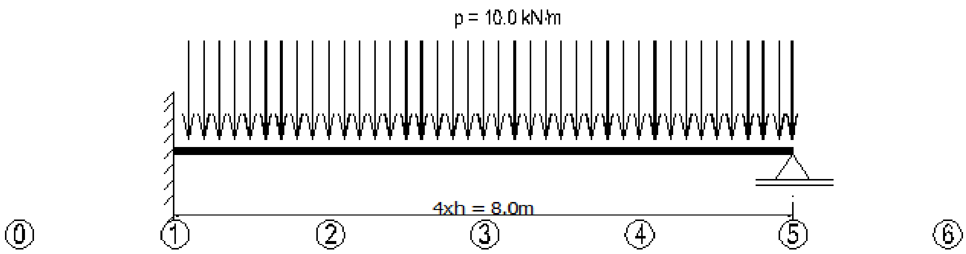

Figure 14. Uniform fixed–pinned beam subjected to a uniformly distributed load.

 doi:10.20944/preprints202105.0252.v1

The governing equations (Equations (10a-b)) are applied at grid points 1, 2, 3, 4, and 5. The boundary conditions are satisfied using Equation (11a).

The bending shear factor $\alpha = EI/\kappa GAl^2 = 0.025$ (Equation (9c))

In this study, analysis was conducted with the W–Φ FDM, M–W FDM, and W FDM approximations. Details of the analysis and results are presented in Appendix A and in the Supplementary Material "Fixed–pinned beam subjected to a uniformly distributed load". Table 1 lists the results obtained with classical beam theory (CBT) and those obtained with W–Φ FDM and M–W FDM approximations. Table 2 lists the results obtained with classical beam theory (CBT) and those obtained with W FDM approximation.

Table 1. Bending moments (kNm) in the beam for a number of grid points: classical beam theory (CBT) and present study (W–Φ FDM and M–W FDM approximations).

Position X(m)	**CBT (exact results)**	**Present study 5-point grid**		**Present study 9-point grid**		**Present study 13-point grid**	
		W–Φ	**M–W**	**W–Φ**	**M–W**	**W–Φ**	**M–W**
0.0	-74.42	-50.07	-67.80	-65.89	-72.73	-70.33	-73.66
2.0	4.19	-0.63	9.15	2.47	5.45	3.36	4.75
4.0	42.79	24.20	46.10	36.24	43.64	39.64	43.17
6.0	41.40	24.41	43.05	35.42	41.82	38.52	41.58
8.0	0.00	0.00	0.00	0.00	0.00	0.00	0.00

Although the results of both approximations converge toward the exact results, the M–W approximation delivers better results than the W–Φ approximation for a given grid. Accuracy increases with an increasing number of grid points. The M–W FDM approximation yields better results of bending moments than the W–Φ FDM approximation, since results are obtained here through a one-step approximation, whereas results by the W–Φ FDM approximation are obtained through a two-step approximation (w and φ are determined in the first step, and the moment M is calculated in the second step).

Table 2. Bending moments (kNm) in the beam for a number of grid points: classical beam theory (CBT) and present study (W FDM approximation).

Position X(m)	**CBT (exact results)**	**Present study 5-point grid W FDM**	**Present study 3-point grid W FDM**	**Present study 2-point grid W FDM**
0.0	-74.42	-74.42	-74.42	-74.42
2.0	4.19	4.19		
4.0	42.79	42.79	42.79	
6.0	41.40	41.40		
8.0	0.00	0.00	0.00	0.00

The results obtained with the W FDM approximation are exact for a uniformly distributed load regardless of the discretization, since the exact solution for the deflection curve here is a fourth-order polynomial, which corresponds to the FDM approximation.

3.1.2 Beam subjected to a concentrated load

We analyzed a uniform fixed–pinned beam subjected to a concentrated load, as shown in Figure 15.

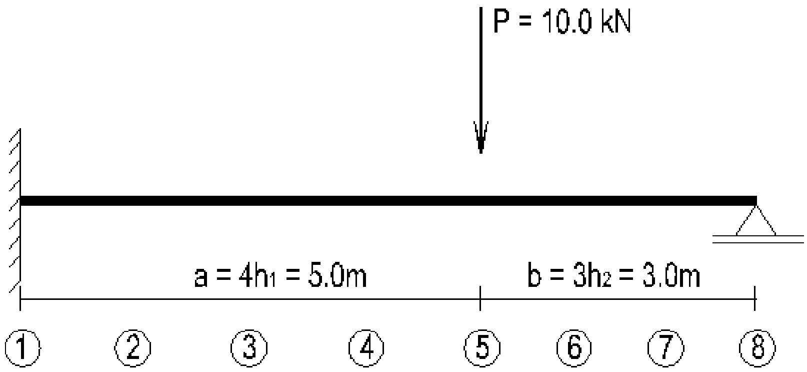

Figure 15. Uniform fixed–pinned beam subjected to a concentrated load

The models showing the grid points (Figure 4a,b and Figure 5a,b) are considered.

In this study, analysis was conducted with the W–Φ FDM, M–W FDM, and W FDM approximations. Details of the analysis and results are presented in Appendix B and in the Supplementary Material “Fixed–pinned beam subjected to a concentrated load.” Table 3 lists the results obtained with classical beam theory (CBT) and those obtained in this study (W–Φ FDM, M–W FDM, and W FDM approximations).

Preprints (www.preprints.org) | NOT PEER-REVIEWED | Posted: 11 May 2021 doi:10.20944/preprints202105.0252.v1

Table 3. Bending moments (kNm) in the beam: classical beam theory (CBT) and present study (W–Φ FDM, M–W FDM, and W FDM approximations).

Position X(m)	**CBT (exact results)**	**Eight-point grid (4 × 1.25 m) + (3 × 1.0 m)**		**Eight-point grid (4 × 1.25 m) + (3 × 1.0 m)**	**Three-point grid 5.0 m + 3.0 m**
		W–Φ FDM	**M–W FDM**	**W FDM**	**W FDM**
0.00	-12.16	-11.96	-11.80	-12.16	-12.16
1.25	-5.57	-5.41	-5.27	-5.57	
2.50	1.01	1.15	1.26	1.01	
3.75	7.60	7.71	7.79	7.60	
5.00	14.19	14.26	14.33	14.19	14.19
6.00	9.46	9.51	9.55	9.46	
7.00	4.73	4.75	4.78	4.73	
8.00	0.00	0.00	0.00	0.00	0.00

The results obtained with W–Φ FDM and M–W FDM approximations have gut accuracy. Surprisingly, the W–Φ approximation here delivers better results than the M–W approximation. The results obtained with the W FDM approximation are exact for a concentrated load regardless of the discretization, since the exact solution for the deflection curve here is a third-order polynomial, which is exactly described with the fourth-order polynomial FDM approximation.

3.1.3 Tapered pinned–fixed beam subjected to a uniformly distributed load

We analyzed a tapered pinned–fixed beam subjected to a uniformly distributed load, as shown in Figure 16.

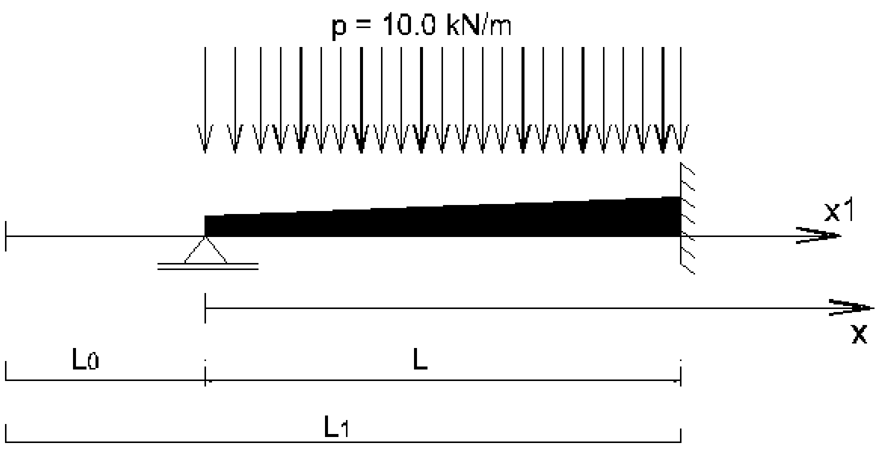

Figure 16. Tapered pinned–fixed beam subjected to a uniformly distributed load.

Preprints (www.preprints.org) | NOT PEER-REVIEWED | Posted: 11 May 2021 doi:10.20944/preprints202105.0252.v1

At position x_1 of the beam, the second moment of area I($x1$) and the cross-sectional area A(x_1) are defined as follows:

$$I(x_1) = I_1 \left(x_1 / L_1 \right)^4 \tag{65a}$$

$$A(x_1) = A_1 \left(x_1 / L_1 \right)^2 \tag{65b}$$

where I_1 and A_1 are the second moment of area and the cross-sectional area at the fixed end $x_1 = L_1$, respectively.

L = 8.0 m, L_0 = 2.0 m, and α_r = 0.020.

First, the beam is calculated using the force method of classical beam theory (exact results). Then, the calculation is conducted with the FDM using n = 9, 17, and 25 grid points. Details of the analysis and results are presented in Appendix C and in the Supplementary Material “Tapered pinned–fixed beam subjected to a uniformly distributed load.” Table 4 lists the results obtained with classical beam theory (the exact results) and those obtained in this study (W–Φ FDM and M–W FDM approximations).

Table 4. Bending moments (kNm) in the beam for a number of grid points: classical beam theory (CBT) and present study **(**W–Φ FDM and M–W FDM approximation**s**).

Position X(m)	**CBT (exact results)**	**Present study 9-point grid**		**Present study 17-point grid**		**Present study 25-point grid**	
		W–Φ	**M–W**	**W–Φ**	**M–W**	**W–Φ**	**M–W**
0.00	0.00	0.00	0.00	0.00	0.00	0.00	0.00
1.00	13.77	6.88	14.00	12.34	13.80	13.52	13.78
2.00	17.53	21.76	18.00	20.90	17.61	19.54	17.56
3.00	11.30	23.55	12.01	16.90	11.41	13.84	11.34
4.00	-4.93	12.95	-3.99	-0.69	-4.79	-3.50	-4.88
5.00	-31.17	-16.51	-29.99	-30.94	-30.99	-31.93	-31.10
6.00	-67.40	-64.15	-65.99	-72.91	-67.18	-71.03	-67.32
7.00	-113.64	-127.95	-111.99	-125.90	-113.38	-120.51	-113.54
8.00	-169.87	-205.89	-167.98	-189.48	-169.58	-180.21	-169.76

Although the results of both approximations converge toward the exact results, the M–W approximation delivers better results than the W–Φ approximation for a given grid. Accuracy increases with an increasing number of grid points. The M–W FDM approximation yields better results of bending moments than the W–Φ FDM approximation, since results are obtained here through a one-step approximation, whereas results by the W–Φ FDM approximation are obtained through a two-step approximation (w and φ are determined in the first step, and the moment M is calculated in the second step).

3.2 Second-order analysis

3.2.1 Beam subjected to a uniformly distributed load and a compressive force

We analyzed a uniform pinned–pinned beam subjected to a uniformly distributed load and a compressive force, as shown in Figure 17.

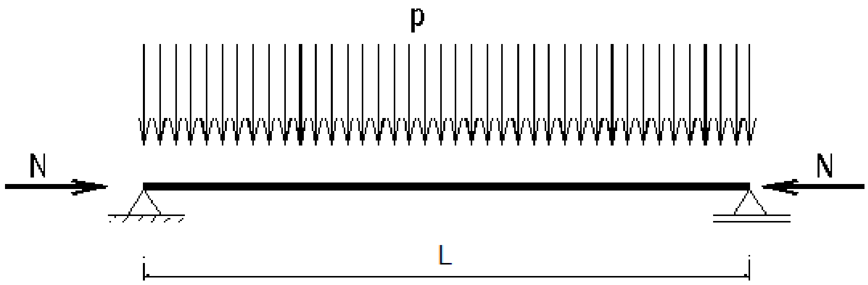

Figure 17. Pinned–pinned beam subjected to a uniformly distributed load and a compressive force.

$Nl^2 / EI =$ -3.00, p = 10.0 kN/m, l = 8.0 m α = EI/κGAl² = 0.02.

Fogang [6] presented a closed-form expression of the bending moment in a pinned–pinned beam. In this study, the analysis is conducted with n = 9, 17, and 25 grid points. Details of the analysis and results are presented in the Supplementary Material "Pinned–pinned beam subjected to a uniformly distributed load and compressive force." Table 5 lists the results obtained by Fogang [6] and those obtained in this study (W–Φ FDM, M–W FDM, and W FDM approximations).

Table 5. Bending moments (kNm) in a pinned–pinned beam: Fogang [6], W–Φ FDM, M–W FDM, and W FDM.

Position X(m)	Fogang [6]	FDM 9-point grid			FDM 17-point grid		
		W–Φ	**M–W**	**W FDM**	**W–Φ**	**M–W**	**W FDM**
0.00	0.00	0.00	0.00	0.00	0.00	0.00	0.00
1.00	54.68	44.11	57.60	55.36	51.59	55.41	54.85
2.00	95.84	77.05	100.96	97.05	90.33	97.11	96.14
3.00	121.39	97.41	127.89	122.95	114.35	123.01	121.78
4.00	130.06	104.29	137.02	131.73	122.49	131.79	130.47

Position X(m)	**Fogang [6]**	**FDM 25-point grid**		
		W–Φ	**M–W**	**W FDM**
0.00	0.00	0.00	0.00	0.00
1.00	54.68	53.26	55.00	54.76
2.00	95.84	93.31	96.40	95.97
3.00	121.39	118.16	122.11	121.56
4.00	130.06	126.58	130.83	130.24

The results of this study have high accuracy.

3.2.2 Buckling load of a fixed–pinned beam

We determined the buckling load of a fixed–free beam, as shown in Figure 18.

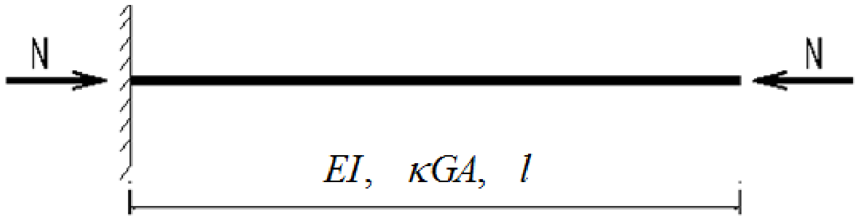

Figure 18. Buckling load of a fixed–free beam.

In this study, analysis was conducted with n = 9 and 17 grid points. The buckling load N_{cr} is defined as follows:

$$N_{cr} = -\pi^2 EI/(\beta l)^2 \tag{66}$$

Hu et al. [5] presented the following closed-form expression of the buckling load of a fixed–free beam:

$$N_{cr} = \frac{-\pi^2 EI}{4l^2\left(1+\pi^2\varphi/48\right)} \qquad \varphi = \frac{12EI}{l^2\kappa GA} \tag{67a}$$

The combination of Equations (9c), (66), and (67a) yields the buckling factor β as follows:

$$\beta = \sqrt{4+\pi^2\varphi/12} \equiv \sqrt{4+\pi^2\alpha} \tag{67b}$$

Details of the analysis and results are presented in the Supplementary Material "Buckling load of a fixed–free beam." Table 6 lists the results obtained by Hu et al. [5] and those obtained in this study (W–Φ, M–W, and W FDM approximations) for different values of the bending shear factor α (Equation (9c)).

Table 6. Buckling factors β of the beam: Hu et al. [5], W–Φ FDM, M–W FDM, and W–FDM.

α = EI/κGAl²	Hu et al. [5]	FDM 9-point grid			FDM 17-point grid		
		W–Φ	**M–W**	**W FDM**	**W–Φ**	**M–W**	**W FDM**
0.0250	2.0608	2.1049	2.0639	2.0711	2.0719	2.0615	2.0634
0.0500	2.1198	2.1429	2.1228	2.1301	2.1260	2.1205	2.1224
0.0750	2.1772	2.1943	2.1802	2.1875	2.1817	2.1779	2.1798
0.1000	2.2332	2.2471	2.2360	2.2425	2.2368	2.2339	2.2357

The results of this study have high accuracy.

3.2.3 Second-order element stiffness matrix of a uniform beam

Let us calculate the element stiffness matrix of a beam with the following characteristics:

k = -1.5 (Equation (42c)), α = 0.05 (Equation (9c)), and length L = 4.0 m.

The matrix is calculated with W FDM and M–W FDM approximations. The stiffness matrix is as follows:

$$K_{Tbl} = EI \times \begin{bmatrix} T_{TB} & Q_{TB} & -T_{TB} & Q_{TB} \\ & S_{TB} & -Q_{TB} & C_{TB} \\ & & T_{TB} & -Q_{TB} \\ sym. & & & S_{TB} \end{bmatrix} \tag{68}$$

Let us now calculate the stiffness matrix of the beam with the following formula presented by Hu et al. [5]:

$$K_{Tbl} = EI\chi \times \begin{bmatrix} 0 & 0 & (\lambda/L)^2 & 0 \\ (\lambda/L)^2 & 0 & 0 & 0 \\ 0 & 0 & -(\lambda/L)^2 & 0 \\ -(\lambda/L)^2\cos\lambda & -(\lambda/L)^2\sin\lambda & 0 & 0 \end{bmatrix} \times \begin{bmatrix} 1 & 0 & 0 & 1 \\ 0 & \chi\lambda/L & 1 & 0 \\ \cos\lambda & \sin\lambda & L & 1 \\ -\chi\lambda/L\sin\lambda & \chi\lambda/L\cos\lambda & 1 & 0 \end{bmatrix}^{-1}$$

The aforementioned characteristics become P = 1.5 × EI/L², χ = 1- P/(ksGA) = 1- 1.5 × 0.05 = 0.925,

$$\lambda = \sqrt{PL^2/\chi EI} = \sqrt{1.5/0.925} = 1.273$$

Details of the results are presented in Appendix D and in the Supplementary Material "Second-order element stiffness matrix of a uniform beam." Table 7 lists the results obtained by Hu et al. [5] and those obtained in this study (M–W FDM

Preprints (www.preprints.org) | NOT PEER-REVIEWED | Posted: 11 May 2021 doi:10.20944/preprints202105.0252.v1

and W FDM approximations). The W–Φ approximation can be considered using appropriate formulas developed in Section 2.2.1.1.

Table 7. Second-order element stiffness matrix: Hu et al. [5], M–W FDM, and W FDM.

	Hu et al. [5]	**9-point grid**		**13-point grid**		**17-point grid**	
		M–W	**W FDM**	**M–W**	**W FDM**	**M–W**	**W FDM**
T_{TB}	0.0917	0.0897	0.0913	0.0908	0.0915	0.0912	0.0916
Q_{TB}	0.2303	0.2263	0.2295	0.2285	0.2300	0.2293	0.2301
S_{TB}	0.6759	0.6682	0.6767	0.6725	0.6763	0.6740	0.6761
C_{TB}	0.2454	0.2369	0.2465	0.2416	0.2459	0.2432	0.2457

The results of this study have high accuracy.

3.3.1 Free vibration analysis of a fixed–free beam

We determined the vibration frequencies of a fixed–free beam. Analysis was conducted with n = 9, 17, and 25 grid points. Details of the analysis and results are listed in Appendix E and in the Supplementary Material "Vibration analysis of a uniform fixed–free beam." The vibration frequency coefficients λ are defined in Equation (52b). The results (depending on the bending shear factor and the coefficient of rotary inertia) obtained in this study are compared to those obtained by Kruszewski [15], and are listed in Table 8.

Table 8. Coefficients λ of natural frequencies (first mode) of a fixed–free beam.

α/k_{RI}	**Kruszewski [15]**	**Present study 9-point grid**		**Present study 17-point grid**		**Present study 25-point grid**	
		W–Φ	**M–W**	**W–Φ**	**M–W**	**W–Φ**	**M–W**
0.025 / 0.010	3.2662	3.4917	3.2290	3.3245	3.2568	3.2922	3.2620
0.025 / 0.015	3.2368	3.4549	3.2005	3.2933	3.2276	3.2621	3.2327
0.050 / 0.010	3.1159	3.2226	3.0833	3.1431	3.1077	3.1280	3.1122
0.050 / 0.015	3.0927	3.1967	3.0607	3.1192	3.0847	3.1045	3.0891

The results of this study have high accuracy.

 doi:10.20944/preprints202105.0252.v1

3.3.2 Free vibration analysis of beams resting on Winkler foundation and subjected to a compression force

We determined the dynamic response of beams subjected to an axial load. An elastic Winkler foundation was also considered. A pinned–pinned and a fixed–pinned beam were analyzed.

Ghannadiasl [14] analytically solved the case of beams with various boundary conditions, resting on an elastic Winkler foundation and subjected to an axial load. The beams have the following characteristics: Poisson's ratio $\nu = 0.25$, Timoshenko shear coefficient $\kappa = 2/3$, and coefficient of rotary inertia $k_{RI} = 0.01$.

$$\alpha = \frac{EI}{\kappa GAL^2} = \frac{1}{\kappa} \times \frac{E}{G} \times \frac{I}{AL^2} = \frac{1}{2/3} \times 2 \times (1+0.25) \times 0.01 = 0.0375$$

$$N_x = -0.6 \times \pi^2 \times \frac{EI}{L^2} \qquad \rightarrow k_N = -5.922$$

The definition of the stiffness of the Winkler foundation in Ghannadiasl [14] has an error: in the denominator, the expression should be L^4 instead of L^2.

Analysis was conducted with n = 9, 17, and 33 grid points. Detailed results are listed in the Supplementary Materials "Vibration analysis of a pinned–pinned beam with an axial load" and "Vibration analysis of a fixed–pinned beam with an axial load". Table 9 and Table 10 list the results of Ghannadiasl [14] and those obtained in this study (W–Φ and M–W approximations).

Table 9. Coefficients λ of natural frequencies (first mode) of a pinned–pinned Timoshenko beam under axial load: Ghannadiasl [14], W–Φ, and M–W.

kw	Ghannadiasl [14]	Present study 9-point grid		Present study 17-point grid		Present study 33-point grid	
		W–Φ	M–W	W–Φ	M–W	W–Φ	M–W
0	3.46648	4.26106	3.35291	3.68461	3.43818	3.52250	3.45941
$0.2\times\pi^4$	5.52398	6.05742	5.45397	5.66425	5.50725	5.55952	5.51958
$0.4\times\pi^4$	7.00019	7.43094	6.94550	7.11207	6.98642	7.02844	6.99674
$0.6\times\pi^4$	8.21469	8.58696	8.16850	8.31083	8.20306	8.23893	8.21178
$0.8\times\pi^4$	9.27091	9.60434	9.23034	9.35672	9.26062	9.29253	9.26835

Preprints (www.preprints.org) | NOT PEER-REVIEWED | Posted: 11 May 2021 doi:10.20944/preprints202105.0252.v1

Table 10. Coefficients λ of natural frequencies (first mode) of a fixed–pinned Timoshenko beam under axial load: Ghannadiasl [14], W–Φ, and M–W.

kw	Ghannadiasl [14]	Present study 9-point grid		Present study 17-point grid		Present study 33-point grid	
		W–Φ	M–W	W–Φ	M–W	W–Φ	M–W
0	7.32425	7.86512	7.09499	7.46801	7.26653	7.36077	7.30979
$0.2\times\pi^4$	8.50792	8.98023	8.31146	8.63265	8.45830	8.53955	8.49549
$0.4\times\pi^4$	9.54555	9.97105	9.37093	9.65748	9.50137	9.57390	9.53447
$0.6\times\pi^4$	10.4806	10.87162	10.32186	10.58318	10.44038	10.50656	10.47050
$0.8\times\pi^4$	11.3384	11.70279	11.19194	11.43386	11.30131	11.36259	11.32913

The results of this study have high accuracy.

3.3.3. Free vibration analysis of tapered Timoshenko beams

We determined the vibration frequencies (coefficients λ) of tapered Timoshenko beams. Pinned–pinned, fixed–free, and fixed–fixed beams were considered.

The beams have the following characteristics: Poisson's ratio ν = 0.30, Timoshenko shear coefficient κ = 5/6, and coefficient of rotary inertia k_{RI} = 0.01.

$$\alpha = \frac{EI}{\kappa GAL^2} = \frac{1}{\kappa}\times\frac{E}{G}\times\frac{I}{AL^2} = \frac{1}{5/6}\times 2(1+0.30)\times 0.01 = 0.0312$$

Analysis was conducted with n = 9, 17, 25, 33, and 41 grid points for different values of the taper ratio ($1-h_r/h_l$) and support conditions: h_l and h_r are heights at the left and the right beam's end, respectively. The reference values Ar and Ir are taken at the left beam's end. Detailed results are listed in the Supplementary Material "Vibration analysis of tapered Timoshenko beams." Soltani [16] presented results obtained with the power series method (PSM) and those obtained by Hibbitt et al. [17] with the finite element method using ABAQUS software. The results of this study are compared with their results in Table 11.

Preprints (www.preprints.org) | NOT PEER-REVIEWED | Posted: 11 May 2021 doi:10.20944/preprints202105.0252.v1

Table 11. Coefficients λ of natural frequencies (first mode) of tapered Timoshenko beams: power series method (PSM), ABAQUS, and FDM.

Taper ratio	PSM	ABAQUS	FDM 9-pt grid	FDM 17-pt grid	FDM 25-pt grid	FDM 33-pt grid	FDM 41-pt grid
Fixed–free beam							
0.2	3.3307	3.3770	3.4978	3.3734	3.3498	3.3414	3.3375
0.5	3.5591	3.6890	3.6839	3.5895	3.5725	3.5666	3.5639
Pinned–pinned beam							
0.2	7.7160	7.7370	8.2013	7.8419	7.7723	7.7478	7.7364
0.5	6.4442	6.4740	7.0314	6.5924	6.5100	6.4812	6.4678
Fixed–fixed beam							
0.2	13.2223	13.2380	13.7840	13.3733	13.2903	13.2607	13.2469
0.5	11.9235	11.9500	12.8356	12.1781	12.0392	11.9891	11.9657

The results of this study have high accuracy.

3 Conclusions

The FDM-based model developed in this paper enables, with relative easiness, first-order, second-order, and vibration analyses of Timoshenko beams. The results show that the calculations, as described in this paper, yield accurate results. First- and second-order element stiffness matrices (tensile or compressive axial force) in local coordinates were determined. In addition, tapered beams were analyzed.

The following aspects were not addressed in this study but could be analyzed with the model in the future:

- ✓ Analysis of linear structures, such as frames, through the transformation of element stiffness matrices from local coordinates to global coordinates
- ✓ Second-order analysis of frames free to sidesway, the P-Δ effect being examined
- ✓ Timoshenko beams resting on Pasternak foundations
- ✓ Elastically connected multiple-beam system
- ✓ Axially functionally graded beams.

Supplementary Materials: The following files were uploaded during submission:

- “Fixed–pinned beam subjected to a uniformly distributed load”
- “Fixed–pinned beam subjected to a concentrated load”

- "Tapered pinned–fixed beam subjected to a uniformly distributed load"
- "Pinned–pinned beam subjected to a uniformly distributed load and compressive force"
- "Buckling load of a fixed–free beam"
- "Second-order element stiffness matrix of a uniform beam"
- "Vibration analysis of a uniform fixed–free beam
- "Vibration analysis of a pinned–pinned beam with an axial load"
- "Vibration analysis of a fixed–pinned beam with an axial load"
- "Vibration analysis of tapered Timoshenko beams"

Author Contributions:

Funding:

Acknowledgments:

Conflicts of Interest: The author declares no conflict of interest.

Appendix A: Uniform fixed–pinned beam subjected to a uniformly distributed load

A uniform beam (Figure 14) subjected to a uniformly distributed load was analyzed using the force method of classical beam theory. The bending moment at the fixed end was the redundant effort.

In the associated statically determinate system, $M_0(x)$ and $V_0(x)$ are the bending moment and the shear force, respectively, due to the distributed load, whereas m(x) and v(x) are the bending moment and the shear force, respectively, due to the virtual unit moment at the fixed end. $M_0(x)$, $V_0(x)$, m(x), and v(x) can be expressed as follows:

$$\begin{aligned} M_0(x) &= px(l-x)/2 = pl^2\xi(1-\xi)/2 \qquad & m(x) &= 1 - x/l = 1-\xi \\ V_0(x) &= p(l/2-x) = pl(1/2-\xi) & v(x) &= -1/l \end{aligned} \tag{A1}$$

The bending moment M_1 at the fixed end is the solution of the following equations:

$$\delta_{10} = \int_0^l \frac{M_0(x)\times m(x)}{EI}dx + \int_0^l \frac{V_0(x)\times v(x)}{\kappa GA}dx \rightarrow EI\delta_{10} = \frac{pl^3}{24} + 0 \tag{A2}$$

$$\delta_{11} = \int_0^l \frac{m(x)\times m(x)}{EI}dx + \int_0^l \frac{v(x)\times v(x)}{\kappa GA}dx \rightarrow EI\delta_{11} = \frac{l}{3} + l\frac{EI}{\kappa GAl^2} \tag{A3}$$

$$M_1 = -\frac{\delta_{10}}{\delta_{11}} = -\frac{pl^2}{8 + 24\dfrac{EI}{\kappa GAl^2}} \tag{A4}$$

Preprints (www.preprints.org) | NOT PEER-REVIEWED | Posted: 11 May 2021 doi:10.20944/preprints202105.0252.v1

Combining Equations (A1) and (A4) yields the bending moment at any position *x*, as follows:

$$M(x) = M_0(x) + M_1 \times m(x) \tag{A5}$$

Appendix B: Uniform fixed–pinned beam subjected to a concentrated load

A uniform beam (Figure 15) subjected to a concentrated load was analyzed using the force method of classical beam theory. The bending moment at the fixed end was the redundant effort.

Analysis was conducted similarly to the example in Appendix A.

$$EI\delta_{10} = \frac{1}{6}Pab\left(1 + b/l\right) + 0 \qquad EI\delta_{11} = \frac{l}{3} + l\frac{EI}{\kappa GAl^2} \tag{B1}$$

$$M_1 = -\frac{\delta_{10}}{\delta_{11}} = -\frac{Pab\left(1+b/l\right)}{l\left(2 + 6\dfrac{EI}{\kappa GAl^2}\right)}$$

Appendix C: Tapered pinned–fixed beam subjected to a uniformly distributed load

A tapered beam (Figure 16) subjected to a uniformly distributed load was analyzed using the force method of classical beam theory. The bending moment at the fixed end was the redundant effort.

In the associated statically determinate system, $M_0(x)$ and $m(x)$ are the bending moments due to the distributed load and the virtual unit moment at the fixed end, respectively. $V_0(x)$ and $v(x)$ are the shear forces due to the distributed load and the virtual unit moment at the fixed end, respectively. Let us introduce the dimensionless ordinate $\xi = x/l$ and $\xi_0 = L_0/L_1$. $M_0(x)$, $V_0(x)$, $m(x)$, $v(x)$, $I(x)$, and $A(x)$ can be expressed as follows:

$$\begin{aligned}
&M_0(x) = px(l-x)/2 = pl^2\xi(1-\xi)/2 \qquad && m(x) = x/l = \xi \\
&V_0(x) = p(l/2 - x) = pl(1/2-\xi) && v(x) = 1/l \\
&I(x) = I_1\left(x_1/L_1\right)^4 = I_1\left[\xi_0 + \xi(1-\xi_0)\right]^4 \\
&A(x) = A_1\left(x_1/L_1\right)^2 = A_1\left[\xi_0 + \xi(1-\xi_0)\right]^2
\end{aligned} \tag{C1}$$

Applying Equations (A2) and (A3), the bending moment M_1 at the fixed end is the solution of the following equations:

$$EI_1\delta_{10} = \frac{pl^3}{2} \times \int_0^1 \frac{\xi^2(1-\xi)}{\left[\xi_0 + \xi(1-\xi_0)\right]^4} d\xi + \alpha_r pl^3 \times \int_0^1 \frac{(1/2-\xi)}{\left[\xi_0 + \xi(1-\xi_0)\right]^2} d\xi \tag{C2}$$

$$EI_1\delta_{11} = l \times \int_0^1 \frac{\xi^2}{\left[\xi_0 + \xi(1-\xi_0)\right]^4} d\xi + \alpha_r l \int_0^l \frac{1}{\left[\xi_0 + \xi(1-\xi_0)\right]^2} d\xi \tag{C3}$$

$$M_1 = -\delta_{10}/\delta_{11} \tag{C4}$$

 doi:10.20944/preprints202105.0252.v1

Equations (C2) and (C3) are solved numerically. Combining Equations (A1), (A4), and (A5) yields the bending moment at any position x.

For the analysis of the tapered beam with the FDM, the parameters $\beta'_M(x)$ (Equation (14c)) and $\beta'_V(x)$ (Equation (14d)) are calculated as follows:

$$\beta_M(x)=\left[\xi_0+\xi(1-\xi_0)\right]^4 \rightarrow \beta'_M(x)=h_k\frac{d\beta_M(x)}{dx}=4\beta_{lk}(1-\xi_0)\left[\xi_0+\xi(1-\xi_0)\right]^3 \tag{C5}$$
$$\beta_V(x)=\left[\xi_0+\xi(1-\xi_0)\right]^2 \rightarrow \beta'_V(x)=h_k\frac{d\beta_V(x)}{dx}=2\beta_{lk}(1-\xi_0)\left[\xi_0+\xi(1-\xi_0)\right]$$

Appendix D: Second-order element stiffness matrix of a uniform beam

W FDM approximation

The static compatibility boundary conditions are expressed as follows:

$$T_i=-T_1 \Longrightarrow T_i-(1+k_N\alpha_r)\frac{-W_{-1}+2W_0-2W_2+W_3}{2h_k^3}+\beta_{lk}^2k_N\frac{W_{-1}-8W_0+8W_2-W_3}{12h_k^3}=0$$
$$M_i=M_1 \rightarrow M_i+(1+k_N\alpha_r)\frac{-W_{-1}+16W_0-30W_1+16W_2-W_3}{12h_k^2}=0 \tag{D1}$$
$$T_k=T_{n+1} \Longrightarrow T_k+(1+k_N\alpha_r)\frac{-W_{n-1}+2W_n-2W_{n+2}+W_{n+3}}{2h_k^3}-\beta_{lk}^2k_N\frac{W_{n-1}-8W_n+8W_{n+2}-W_{n+3}}{12h_k^3}=0$$
$$M_k=-M_{n+1} \rightarrow M_k-(1+k_N\alpha_r)\frac{-W_{n-1}+16W_n-30W_{n+1}+16W_{n+2}-W_{n+3}}{12h_k^2}=0$$

The geometric compatibility boundary conditions are expressed as follows:

$$W_1=EI_rw_i \tag{D2}$$
$$EI_r\varphi_1=\frac{\alpha_r}{\beta_{lk}^2}(1+k_N\alpha_r)\frac{-W_{-1}+2W_0-2W_2+W_3}{2h_k}+\frac{W_{-1}-8W_0+8W_2-W_3}{12h_k}=EI_r\varphi_i$$
$$W_{n+1}=EI_rw_k$$
$$EI_r\varphi_{n+1}=\frac{\alpha_r}{\beta_{lk}^2}(1+k_N\alpha_r)\frac{-W_{n-1}+2W_n-2W_{n+2}+W_{n+3}}{2h_k}+\frac{W_{n-1}-8W_n+8W_{n+2}-W_{n+3}}{12h_k}=EI_r\varphi_k$$

 doi:10.20944/preprints202105.0252.v1

M–W FDM approximation

The static compatibility boundary conditions are expressed as follows:

$$
\begin{aligned}
&T_i = -T_1 \Longrightarrow T_i + \frac{h_k^2 M_2 - h_k^2 M_0}{2h_k^3} + \frac{N_i h_k^2}{EI_r}\frac{W_2 - W_0}{2h_k^3} = 0 \\
&M_i = M_1 \rightarrow h_k^2 M_i - h_k^2 M_1 = 0 \\
&T_k = T_{n+1} \Longrightarrow T_k - \frac{h_k^2 M_{n+2} - h_k^2 M_n}{2h_k^3} - \frac{N_i h_k^2}{EI_r}\frac{W_{n+2} - W_n}{2h_k^3} = 0 \\
&M_k = -M_{n+1} \rightarrow h_k^2 M_k + h_k^2 M_{n+1} = 0
\end{aligned}
\tag{D3}
$$

The geometric compatibility boundary conditions are expressed as follows:

$$
\begin{aligned}
&w_1 = w_i \rightarrow W_1 = EI_r \times w_i \\
&\varphi_1 = \varphi_i \rightarrow EI_r \times \varphi_1 = \frac{W_2 - W_0}{2h_k} - \frac{\alpha_r}{\beta_{lk}^2}\frac{h_k{}^2 M_2 - h_k{}^2 M_0}{2h_k} = EI_r \times \varphi_i \\
&w_{n+1} = w_k \rightarrow W_{n+1} = EI_r \times w_k \\
&\varphi_{n+1} = \varphi_k \rightarrow EI_r \times \varphi_{n+1} = \frac{W_{n+2} - W_n}{2h_k} - \frac{\alpha_r}{\beta_{lk}^2}\frac{h_k{}^2 M_{n+2} - h_k{}^2 M_n}{2h_k} = EI_r \times \varphi_k
\end{aligned}
\tag{D4}
$$

Appendix E

Kruszewski [15] presented the following equation (Equation (14) in [15]) for the determination of natural frequencies of a fixed–free beam:

$$
2 - \frac{k_B\left(k_S^2 + k_{RI}^2\right)}{\sqrt{1 - k_S^2 k_{RI}^2 k_B^2}} \sin k_B\beta \sinh k_B\alpha + \left[k_B^2\left(k_S^2 - k_{RI}^2\right)^2 + 2\right] \cos k_B\beta \cosh k_B\alpha = 0
\tag{E1}
$$

where k_B, k_S, k_{RI}, α, and β are defined in [15] in Equations (3a), (3b), (3c), and (5), respectively.

The following equivalences were noted between the parameters considered by Kruszewski [15] and those considered in this study (PS):

$k_S^2 = \alpha$, $k_B = \lambda$, $k_{RI}^2(K) = k_{RI}(PS)$

References

[1] Fogang, V. Euler-Bernoulli Beam Theory: First-Order Analysis, Second-Order Analysis, Stability, and Vibration Analysis Using the Finite Difference Method. Preprints 2021, 2021020559 (doi: 10.20944/preprints202102.0559.v2).

[2] M. Kindelan, M. Moscoso, P. Gonzalez-Rodriguez. Optimized Finite Difference Formulas for Accurate High Frequency Components. Mathematical Problems in Engineering. Volume 2016, Article ID 7860618, 15 pages. http://dx.doi.org/10.1155/2016/7860618

[3] Onyia, M.E.; Rowland-Lato, E.O. Determination of the critical buckling load of shear deformable unified beam. IJET 2018, Vol 10 No 3. DOI: **10.21817/ijet/2018/v10i3/181003026**

[4] Timoshenko, S.P.; Gere, J.M. Theory of Elastic Stability; McGraw-Hill: New York, USA, 1961.

[5] Hu, Z.P.; Pan, W.H.; Tong, J.Z. Exact solutions for buckling and second-order effect of shear deformable Timoshenko beam–columns based on matrix structural analysis. Appl. Sci. 2019, 9(18), 3814. https://doi.org/10.3390/app9183814

[6] Fogang, V. Timoshenko Beam Theory Exact Solution For Bending, Second-Order Analysis, and Stability. Preprints 2020, 2020110457 (doi: 10.20944/preprints202011.0457.v2).

[7] Mwabora, K. O.; Sigey, J. K.; Okelo, J. A.; Giterere, K. A numerical study on transverse vibration of Euler–Bernoulli beam. IJESIT, Volume 8, Issue 3, May 2019

[8] M. Soltani, A. Sistani, B. Asgarian. Free Vibration Analysis of Beams with Variable Flexural Rigidity Resting on one or two Parameter Elastic Foundations using Finite Difference Method. Conference Paper. The 2016 World Congress on The 2016 Structures Congress (Structures16)

[9] S. Boreyri, P. Mohtat, M. J. Ketabdari, A.Moosavi. Vibration analysis of a tapered beam with exponentially varying thickness resting on Winkler foundation using the differential transform method. International Journal of Physical Research, 2 (1) (2014) 10-15. doi: 10.14419/ijpr.v2i1.2152

[10] K. Torabi, H. Afshari, M. Sadeghi, H. Toghian. Exact Closed-Form Solution for Vibration Analysis of Truncated Conical and Tapered Beams Carrying Multiple Concentrated Masses. Journal of Solid Mechanics Vol. 9, No. 4 (2017) pp. 760-782

[11] Fogang, V. An Exact Solution to the Free Vibration Analysis of a Uniform Timoshenko Beam Using an Analytical Approach . Preprints 2021, 2021010501 (doi: 10.20944/preprints202101.0501.v1).

[12] Y. Yesilce, O. Demirdag, S. Catal: Free vibrations of a multi-span Timoshenko beam carrying multiple spring-mass systems. Sadhana Vol. 33, Part 4, August 2008, pp. 385–401. https://doi.org/10.1007/s12046-008-0026-1.

[13] J.T. Katsikadelis. A New Direct Time Integration Method for the Equations of Motion in Structural

Dynamics. Conference Paper · July 2011. Third Serbian (28th Yu) Congress on Theoretical and Applied Mechanics. https://www.researchgate.net/publication/280154205

[14] A. Ghannadiasl: An analytical solution for free vibration of elastically restrained Timoshenko beam on an arbitrary variable Winkler foundation and under axial load. Latin American Journal of Solids and Structures 12 (2015) 2417-2438. http://dx.doi.org/10.1590/1679-78251504

[15] Kruszewski, E. T: Effect of transverse shear and rotary inertia on the natural frequency of a uniform beam. National advisory committee for aeronautics, Technical note 1909 https://ntrs.nasa.gov/search.jsp?R=19930082587

[16] Soltani, M: Vibration characteristics of axially loaded tapered Timoshenko beams made of functionally graded materials by the power series method. Numerical Methods in Civil Engineering. July 2017. DOI:10.29252/nmce.2.1.1

[17] Hibbitt, D., Karlsson, B., Sorensen, P. (2011). Simulia ABAQUS 6. 11 Users' Manual.